Gondwana Research 39 (2016) 96–113

Contents lists available at ScienceDirect

Gondwana Research

journal homepage: www.elsevier.com/locate/gr

Paleomagnetism of the Central Iberian curve's putative hinge: Too many oroclines in the Iberian Variscides

Daniel Pastor-Galán [a,*], Mark J. Dekkers [a], Gabriel Gutiérrez-Alonso [b,c], Daniël Brouwer [a], Thomas Groenewegen [a], Wout Krijgsman [a], Javier Fernández-Lozano [b], Mariano Yenes [b], Fernando Álvarez-Lobato [b]

[a] Paleomagnetic Laboratory "Fort Hoofddijk", Utrecht University, Budapestlaan 17, 3584CD Utrecht, The Netherlands
[b] Departamento de Geología, University of Salamanca, 37008 Salamanca, Spain
[c] Geology and Geography Department, Tomsk State University, Lenin Street 36, Tomsk 634050, Russian Federation

ARTICLE INFO

Article history:
Received 14 March 2016
Received in revised form 10 June 2016
Accepted 30 June 2016
Available online 15 August 2016

Handling Editor: J.G. Meert

Keywords:
Paleomagnetism
Rock magnetism
Orocline
Iberia
Variscan
Remagnetization

ABSTRACT

The Variscan mountain belt in Iberia defines a large "S" shape with the Cantabrian Orocline in the north and the Central Iberian curve, an alleged orocline belt of opposite curvature, to the south. The Cantabrian Orocline is kinematically well constrained, but the geometry and kinematics of the Central Iberian curve are still controversial. Here, we investigate the kinematics of the Central Iberian curve, which plays an important role in the amalgamation of Pangea since it may have accommodated much of the post-collisional deformation. We have performed a paleomagnetic study on Carboniferous granitoids and Cambrian limestones within the hinge of the curve. Our paleomagnetic and rock magnetic results show a primary magnetization in the granitoids and a widespread Carboniferous remagnetization of the limestones. Syn-kinematic granitoids show ca. 70° counter-clockwise rotations consistent with the southern limb of the Cantabrian Orocline. Post-kinematic granitoids and Cambrian limestones show consistent inclinations but very scattered declinations suggesting that they were magnetized coevally to and after the ~70° rotation. Our results show no differential rotations between northern, southern limb and the hinge zone. Therefore, we discard a late Carboniferous oroclinal origin for the Central Iberian curve.

1. Introduction

The latest supercontinent, Pangea, formed after several collisions during the Paleozoic that amalgamated Laurentia, Baltica, Gondwana, Siberia and an assortment of micro-continents to form a global plate (e.g. Nance et al., 2010; Domeier and Torsvik, 2014). Among the many orogens formed during the birth of Pangea, the Variscan–Alleghanian orogen in Europe and North America stands out because of its sinuous geometry. It shows several striking curves in map view: the Alabama (Thomas, 1977); Pennsylvanian (Wise, 2004); New Foundland (O'Brien, 2012); Bohemian (Tait et al., 1996; Edel et al., 2003), Cantabrian (van der Voo, 2004) and the putative Central Iberian curve (Fig. 1; e.g. Staub, 1926; Martínez-Catalán, 2011).

Orogenic curves can be classified according to their kinematics by two end members: (1) primary curves, inherited from physiographic features (e.g. gulfs, embayments) and (2) secondary oroclines, curves that form from a previously linear continental fragment. All intermediate bent orogens are termed as progressive oroclines (Weil and Sussman, 2004; Johnston et al., 2013). Oroclines are widespread in space and time (Rosenbaum, 2014), show varying curvature ranging from a few degrees to as much as 180° (Johnston, 2001), may affect the entire lithosphere (Pastor-Galan et al., 2012a) and may represent up to thousands of kilometers of shortening (Shaw et al., 2016). Most tectonic restorations consider plates as rigid bodies that move across the Earth's surface following the basic principles of plate tectonics (e.g. Stampfli et al., 2013; Domeier and Torsvik, 2014). However, oroclines are the proof that plates are far less rigid through time than reconstructions often assume. Properly identifying oroclines and unraveling their kinematics is therefore essential for accurate and viable tectonic and paleogeographic reconstructions.

The trend of the Variscan–Alleghanian belt in Iberia depicts the well-known Cantabrian Orocline in the north and an orogenic curve of opposite curvature to the south, known as the Central Iberian curve (Fig. 1; Shaw et al., 2012). After its first description in the early 20th century this curve has been largely ignored. Due to lack of exposure, some of the geometry and most of the kinematics of the Central Iberian curve are largely unknown (Pastor-Galan et al., 2015a). Nonetheless, some authors proposed that the Central Iberian curve is a secondary orocline (Martínez-Catalán, 2011, 2012; Shaw et al., 2012). This hypothesis involves hundreds of kilometers of shortening, large-scale strike-slip tectonics and/or the presence of subduction zones, which has drastic

* Corresponding author.
E-mail address: d.pastorgalan@uu.nl (D. Pastor-Galán).

http://dx.doi.org/10.1016/j.gr.2016.06.016
1342-937X/

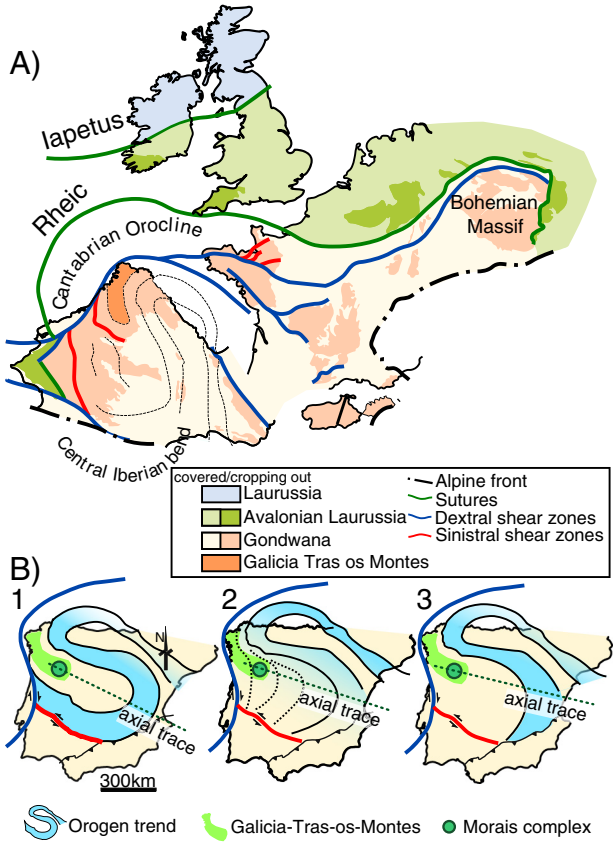

Fig. 1. A) Schematic map of the Variscan belt showing the major terranes, sutures and strike-slip shear zones and the traces of the Cantabrian Orocline and the putative Central Iberian bend. B) Different geometries suggested for the Central Iberian bend, all of them locating the Morais Complex in its core: (1) after Shaw et al., 2012; (2) after Aerden, 2004 and (3) after Martínez-Catalán, 2011.

implications for the amalgamation of Pangea including its configuration and inner stability (Martínez-Catalán, 2011; Shaw et al., 2014; Shaw and Johnston, 2016). In this paper we explore the kinematics of the Central Iberian curve in its core using paleomagnetic analysis. We sampled Carboniferous granitoids around its putative hinge and Cambrian limestones in its southern limb. Our new results indicate that formation of the Central Iberian curve is incompatible with a secondary orocline origin during the late Carboniferous. Therefore, we need an alternative kinematic model to accommodate the observed curve geometry in this part of the Variscan orogen.

2. Overview of the Variscan orogen in Iberia

The Late Paleozoic Variscan orogen of central and western Europe is generally interpreted to be the result of convergence and collision between Laurussia and Gondwana during closure of the Rheic Ocean (e.g. Scotese, 2001; Stampfli and Borel, 2002; Murphy et al., 2006; Nance et al., 2010; Nance et al., 2012; Domeier and Torsvik, 2014). It is one of the major orogenic belts that formed during the amalgamation of Pangea (e.g. Murphy et al., 2009; Stampfli et al., 2013 and references therein).

The Variscan Orogen is classically divided into a number of tectonostratigraphic zones based on fundamental differences in their stratigraphic, structural, magmatic and metamorphic evolution (e.g. Lotze, 1945; Franke, 1989; Martínez-Catalán et al., 2007; Ballevre et al., 2014). These zones record different aspects of the Late Cambrian–Early Ordovician opening of the Rheic Ocean and the migration of terranes from the margin of Gondwana towards Laurussia, as well as the tectonothermal events that accompanied the closure of that ocean. Similarities within individual zones facilitate their correlation along the length of the entire orogenic belt. Relevant to this paper are the Central Iberian Zone – not to be confused with the Central Iberian curve – and Galicia–Tras-os-Montes.

The earliest Variscan deformation in Iberia is interpreted to have occurred prior to c. 400 Ma and its origin is debated (Dallmeyer and Ibarguchi, 1990; Quesada, 1991; Gómez Barreiro et al., 2006; Martínez-Catalán et al., 2009). The first evidences of continental collision, however, occurred later, at ca. 365–370 Ma (Dallmeyer et al., 1997; Rodriguez et al., 2003; López-Carmona et al., 2014) with the underplating of the Gondwanan margin below Laurussia, giving rise to an east-northeastward (in present-day coordinates) migration of deformation, metamorphic and magmatic episodes and syn-orogenic sedimentation (Dallmeyer et al., 1997).

The magmatic history of Central Iberia can be divided into three main episodes: the first episode comprises the so called “Early Granodiorites” (Capdevila and Floor, 1970). Their ages are poorly known, but these granodiorites are interpreted to have intruded at ca. 340 Ma (Gallastegui, 2005). Subsequent “Syn-kinematic” anatectic leucogranites and granodiorites (Capdevila et al., 1973; Castro et al., 2002; López-Plaza et al., 2008; López-Moro et al., 2012) have been dated at ca. 325–318 Ma in NW Iberia (Escuder Viruete et al., 1994; Díez Balda et al., 1995; Escuder Viruete, 1998; Ferreira et al., 2000; Valverde-Vaquero et al., 2007; Costa et al., 2014; Gomes et al., 2014). These intrusive features have been related to large extensional shear zones and are interpreted to reflect the main phase of orogenic collapse (Bea et al., 2006; Castiñeiras et al., 2008). Finally, the “Post-kinematic” granodiorites, dated mostly between ca. 310 and 295 Ma, postdate all Variscan deformation and are coeval with the development of the Cantabrian Orocline. These late granitoids are interpreted to be the result of lithospheric delamination caused by orocline buckling (Gutiérrez-Alonso et al., 2011a, 2011b) or by thermal enhancement in an orogenically thickened continental crust (Bea et al., 2003; Alcock et al., 2009, 2015).

2.1. The Cantabrian Orocline

The Cantabrian Orocline (a.k.a. Ibero–Armorican Arc) is arguably one the best studied oroclines on Earth (e.g. Weil et al., 2013; Gutiérrez-Alonso et al., 2012). It is characterized by a curved structural trend that traces an arc from Brittany across the Bay of Biscay into the Central Iberian zone (Fig. 1). An assortment of geological data support a secondary oroclinal model for the Cantabrian Orocline, in which an originally near-linear Variscan orogenic edifice buckled around a vertical axis (e.g. van der Voo et al., 1997; Kollmeier et al., 2000; Weil et al., 2001; Pastor-Galán et al., 2012b). Orocline formation is constrained to a short period of ca. 10 to 15 Myr between 310 and 295 Ma based on paleomagnetic (Weil et al., 2010), structural (Merino-Tomé et al., 2009; Pastor-Galán et al., 2011; Pastor-Galán et al., 2014; Shaw et al., 2016) and geochronological data (Gutiérrez-Alonso et al., 2015). The closure of the Rheic Ocean resulted in shortening during the Devonian and Carboniferous, which produced a near-linear Variscan orogen. Subsequent change in the shortening direction close to the Carboniferous–Permian boundary resulted in oroclinal buckling (e.g. Weil et al., 2001; Pastor-Galán et al., 2011). Petrologic and isotopic data indicate penecontemporaneous magmatic and tectonothermal activity with the oroclinal buckling over the short 10–15 Myr time window at the end of the Carboniferous (Gutiérrez-Alonso et al., 2011a, 2011b). Orocline formation and large scale intrusions are thought to be part of a single process of lithospheric buckling. Buckling of the entire lithosphere would produce thinning in the outer arc, thickening in the inner arc, and ultimately foundering and delamination of the mantle lithosphere under western Europe (Fernández-Suárez et al., 2002; Gutiérrez-Alonso et al., 2004, 2011a, 2011b), an hypothesis that was successfully tested with analog modeling (Pastor-Galan et al., 2012a).

2.2. The Central Iberian curve

The Cantabrian Orocline is not the only orogenic curve described in the Iberian Variscides. Another arcuate structure of similar magnitude and opposite curvature occurs in the central part of the Iberian Massif. It is known as the Central Iberian curve (Fig. 1) and was described by Staub (1926) for the first time and included in seminal works by Holmes (1929) and Du Toit (1937) (see Martínez-Catalán et al. (2015) for a historical perspective on the Central Iberian curve). Due to the lack of exposure its shape, kinematic and tectonic implications remained ignored for several decades.

In the early 21st century Aerden (2004) brought back the Central Iberian curve hypothesis. Since then, several authors tried to unravel its geometry and kinematics with contradictory results. The new arguments used in support of the Central Iberian curved geometry are: (i) paleocurrents recorded in Ordovician quartzites (Shaw et al., 2012; Fig. 1B-1); (ii) structural trend of folds and inclusions in garnets (Aerden, 2004; Fig. 1B-2) and (iii) aeromagnetic lineations and fold trends (Martínez-Catalán, 2012; Fig. 1B-3). Based on those arguments, three geometries have been proposed (Fig. 1B). All of them share two features: (1) The curvature runs parallel to the Central Iberian Zone, located in the center-west of Iberia and (2) all place the Galicia–Tras-os-Montes Zone in the core of the curve. In all these geometries the Morais Complex, a set of mafic and ultramafic rocks roughly circular in shape (Pin et al., 2006), is cross-cut by the axial trace of the curve (Fig. 1B).

There have been several attempts to explain the kinematics of the curved geometry of the Galicia–Tras-os-Montes and Morais Complexes. Sometimes it has been considered the result of an extrusion wedge product of a non-cylindrical collision (Martínez-Catalán, 1990; Frois da Silva, 2014) or a klippe, a relic of a larger allochtonous thrust sheet (e.g. Rubio Pascual et al., 2013). More recently, Martínez-Catalán (2011) and Shaw et al. (2012, 2016) speculated that both the Cantabrian and Central Iberian zones buckle together as secondary oroclines. Later, Martinez Catalan et al. (2014) reformulated his original hypothesis and proposed that the Central Iberian curve formed as an orocline just before the Cantabrian orocline during a period between 315 and 305 Ma. However, none of these papers contain data that are providing kinematic constraints concerning the timing of the Central Iberian curve. Pastor-Galan et al. (2015a) presented paleomagnetic data from the southern limb of the curve. These authors discard a coeval secondary formation for the Cantabrian orocline and Central Iberian curve and suggest that Central Iberian curve, if real, had to be generated previous to 310 Ma.

3. Local geology

The Central Iberian zone consists of two domains: the "Schist–Greywacke" domain and the "Ollo de Sapo" domain. The Schist–Greywacke Domain, a.k.a. Upright Folds Domain, contains a dominantly terrigenous, marine, Neoproterozoic and early Paleozoic sequence that includes volcanic rocks and granitic orthogneisses (Díez Balda, 1986; Valladares et al., 2000; Rodriguez-Alonso et al., 2004). Variscan deformation started with the development of upright folds (e.g. Díez Balda, 1986), followed by the formation of extensional detachments (Escuder Viruete et al., 1994; Díez Balda et al., 1995). Finally, a third phase of deformation formed strike-slip shear zones and a new phase of upright folding (Díez Balda et al., 1990).

3.1. Tamames syncline

The part of the Central Iberian Zone (CIZ) in the studied area, the so called Upright Folds Domain (Díez Balda et al., 1990), is characterized by: (i) a predominance of Ediacaran and Lower Paleozoic sediments; (ii) a large number of Variscan granitoids intruding these strata; (iii) in the center of the CIZ, NW–SE upright folds that occasionally also preserve Silurian, Devonian and, in some cases, Carboniferous sediments in synclines. One of these synclines, the Valongo–Tamames syncline, extends for more than 250 km along strike from Portugal to the province of Salamanca and is intruded to the east by the Carboniferous Central System Batholith (Yenes et al., 1999). The syncline folds Ediacaran to Devonian sedimentary rocks comprising, from bottom to top, the Aldeatejada, Tamames sandstone, Tamames limestone formations, all of them are overlain uncomformably by the Lower Ordovician Armorican Quartzite followed by other siliciclastic rocks with some interbedded volcanics up to the Middle Devonian (Gutiérrez-Alonso et al., 2008).

Pastor-Galan et al. (2015a) studied paleomagnetic directions from the Early Cambrian Tamames limestone formation (Rölz, 1975; Díez Balda, 1986), which only crops out in the northern limb of the syncline. In that study, authors interpreted the dispersion in declination they found as a remagnetization taking place during a counter-clockwise rotation related to the formation of the Cantabrian Orocline. We have performed rock magnetic analysis of the same sample collection to further examine this rather unconventional interpretation. We have also integrated the directional results from that study in the discussion here.

3.2. Tormes and Martinamor Domes

One of the main features of the Central Iberian Zone is the presence of gneiss domes produced during the main collapse of the Variscan orogenic edifice. The gneiss domes are characterized by the presence of large extensional shear zones and the abundance of syn-kinematic anatectic granitoids (Díez Balda et al., 1995; Escuder Viruete, 1998).

We sampled two gneiss domes (Fig. 2): the Tormes Dome (Martínez, 1977; López-Plaza, 1982; Martínez et al., 1988; López-Plaza and Gonzalo, 1993; Escuder Viruete et al., 1994, 1997; López-Plaza et al., 1999; Viruete et al., 2000) and the Martinamor Dome (Díez Balda, 1981; Díez Balda et al., 1995). Both domes are characterized by an antiformal shape, which folds the structural fabric. They are linked to the km thick, top to the SE, extensional shear zones in which lenticular shaped anatectic granitoids preferentially intruded (Escuder Viruete, 1998; López-Moro et al., 2012). The age of the syn-kinematic granitoids is loosely constrained but U–Pb monazite ages between 329 and 320 Ma were obtained in metasediments of the Tormes and Martinamor Domes (Valverde-Vaquero et al., 2007), and between 325 and 320 Ma in granitoids (Valverde-Vaquero et al., 2007). Zircon U–Pb ages from the continuation of the Tormes Dome to the west, in Portugal, yielded ages of 322 to 316 Ma (Costa et al., 2014; Gomes et al., 2014). A subsequent extensional event in the Tormes Dome is interpreted to have occurred between 317 and 313 Ma (Valverde-Vaquero et al., 2007). Finally, a series of conjugated strike-slip shear zones crosscut all the previous structures at ca. 308 Ma (Ar–Ar in synkinematic mica growths; Gutiérrez-Alonso et al., 2015).

3.3. Post-kinematic granitoids

Widespread in western Iberia are volumetrically large igneous bodies that intruded between ca. 310 and 285 Ma, and thus postdate all Variscan structures (e.g. Gutiérrez-Alonso et al., 2011a). These intrusions are interpreted to be linked to mantle replacement during and the generation of the Cantabrian Orocline (Gutiérrez-Alonso et al., 2011b) or to temperature increase related to crustal thickening and an associated increase in radiogenic heat production (Bea et al., 2003; Alcock et al., 2015). In either case, the post-kinematic granitoids are coeval to the development of the Cantabrian Orocline.

In the study area several post-kinematic igneous bodies have been sampled (Fig. 2):

(1) The Béjar–La Alberca Pluton — This is a large composite pluton dated (ziron U–Pb) at ca. 306 and 308 Ma (Zeck et al., 2007; Gutiérrez-Alonso et al., 2011a). The pluton is composed mostly by quartz–monzonites (Yenes et al., 1999).
(2) Villavieja de Yeltes and Cipérez granites — These plutons have

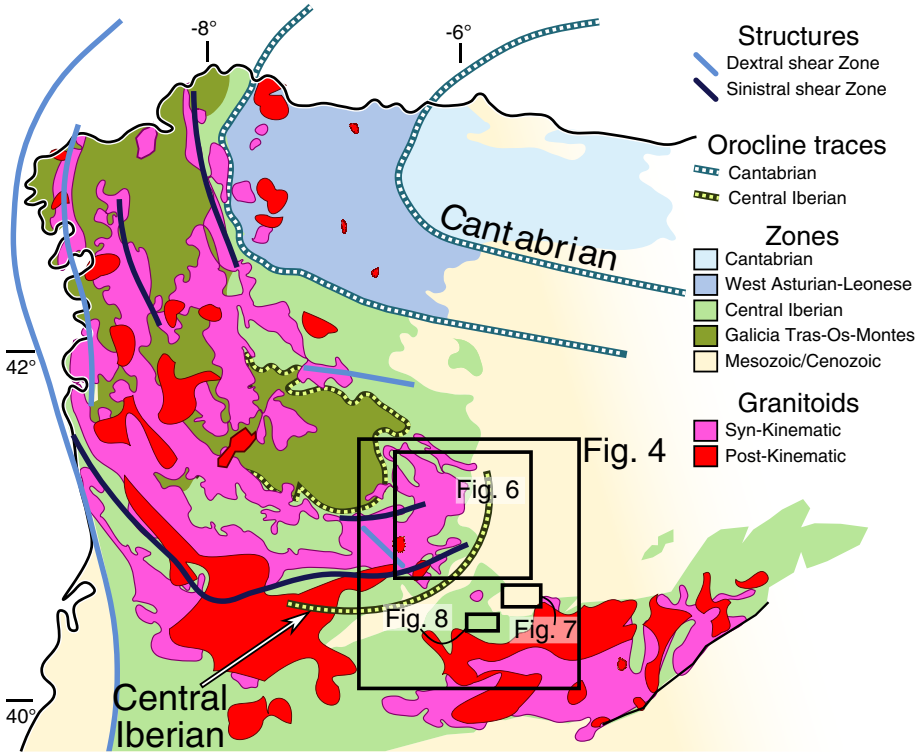

Fig. 2. Simplified map of NW Iberia showing the different tectono-stratigraphic units. Note the curved geometry of the Morais Complex, in the SE tip of the Galicia–Tras-Os-Montes Zone. The map shows the studied areas in squares with numbers referring to the respective detailed figures.

been dated (zircon U–Pb) at ca. 304 and 300 Ma respectively (Gutiérrez-Alonso et al., 2011a, 2011b) and postdate the development of the Juzbado-Traguntia-Penalva do Castelo Shear Zone that bounds the Tormes Dome to the south. The shear zone age is determined at ca. 309 Ma ($^{40}Ar/^{39}Ar$ in biotite; Gutiérrez-Alonso et al., 2015).

(3) Gredos Pluton — In this region, the cristalization age of the post-kinematic granitoids has been constrained with zircon U–Pb ages between ca. 312 and 303 Ma (Zeck et al., 2007; Villaseca et al., 2011; Gutiérrez-Alonso et al., 2011a, 2011b; Orejana et al., 2012; Díaz Alvarado et al., 2013). The samples collected in this pluton include monzogranites, granodiorites, and leucogranites as well as pelitic enclaves.

4. Remanent magnetization directions

4.1. Sampling and laboratory procedures

We drilled a total of 169 cores and 14 blocks, that were obtained from 32 different sites in Carboniferous granitoids (sample_locations.kml file with exact locations is in the Supplementary material). We grouped the sites in localities according to their geological setting: Tormes Dome; Martinamor Dome and post-kinematic granites. We have also performed extensive rock magnetic analysis in 209 cores and 4 blocks from the Tamames Limestones, whose paleomagnetic directions were published in Pastor-Galan et al. (2015a). In the discussion we merge the interpretation of our new results together with those already published.

The natural remanent magnetization (NRM) of samples was investigated through thermal and alternating field (AF) demagnetization. AF demagnetization was carried out using a robotized 2G-SQUID magnetometer, through variable field increments (4–10 mT) up to 70–100 mT. In those samples where high-coercitivity and low-unblocking temperature minerals were expected, we carried out a thermal demagnetization step at 150 °C before AF demagnetization. Stepwise thermal demagnetization was applied with 20–50 °C increments up to complete demagnetization. Principal component analysis (Kirschvink, 1980) was used to calculate magnetic component directions from "Zijderveld" vector end-point demagnetization diagrams (Zijderveld, 1967). Some representative Zijderveld diagrams are shown in Fig. 3. A minimum of 5 points were considered to characterize a remanent direction; directions showing Maximum Anglular Deviation (MAD) over 15° were discarded.

In many of the granitoid samples, NRM components appear to overlap; for such samples we determined remagnetization great circles (Fig. 3). We used the approach of McFadden and McElhinny (1988) in combining great circles and linear best fits (set points). For the interpretation, we only considered great circles passing through previously identified components from vector end-point diagrams (Fig. 3).

Mean directions and uncertainties of each component were evaluated using Fisher statistics of virtual geomagnetic poles (VGPs). Analyses were carried out with the open-source software paleomagnetism.org (Koymans et al., 2016). We applied the sample number (N)-dependent A_{95} envelope of Deenen et al. (2011) to assess the quality and reliability of the different component distributions. These criteria evaluate the scatter of VGPs facilitating its interpretation. In general, if scatter is -mostly- due to paleosecular variation (PSV) of the geomagnetic field, the associated VGP distribution has to be circular and A_{95} will be within certain minimum and maximum values, i.e. $A_{95}min \leq A_{95} \leq A_{95}max$. However, if an important other source of scatter is present such as structural problems, vertical axis rotation or inclination shallowing, VGP distributions will be elongated instead of circular. If in such a case A_{95} becomes larger than $A_{95}max$, then traditional statistical parameters (Fisherian mean, uncertainties, poles) are not representative of the dataset. Finally, if A_{95} is smaller than $A_{95}min$, the scatter underrepresents paleosecular variation or other sources of noise. This may indicate NRM acquisition over a short time period (e.g. a lava flow) or inappropriate sampling. On

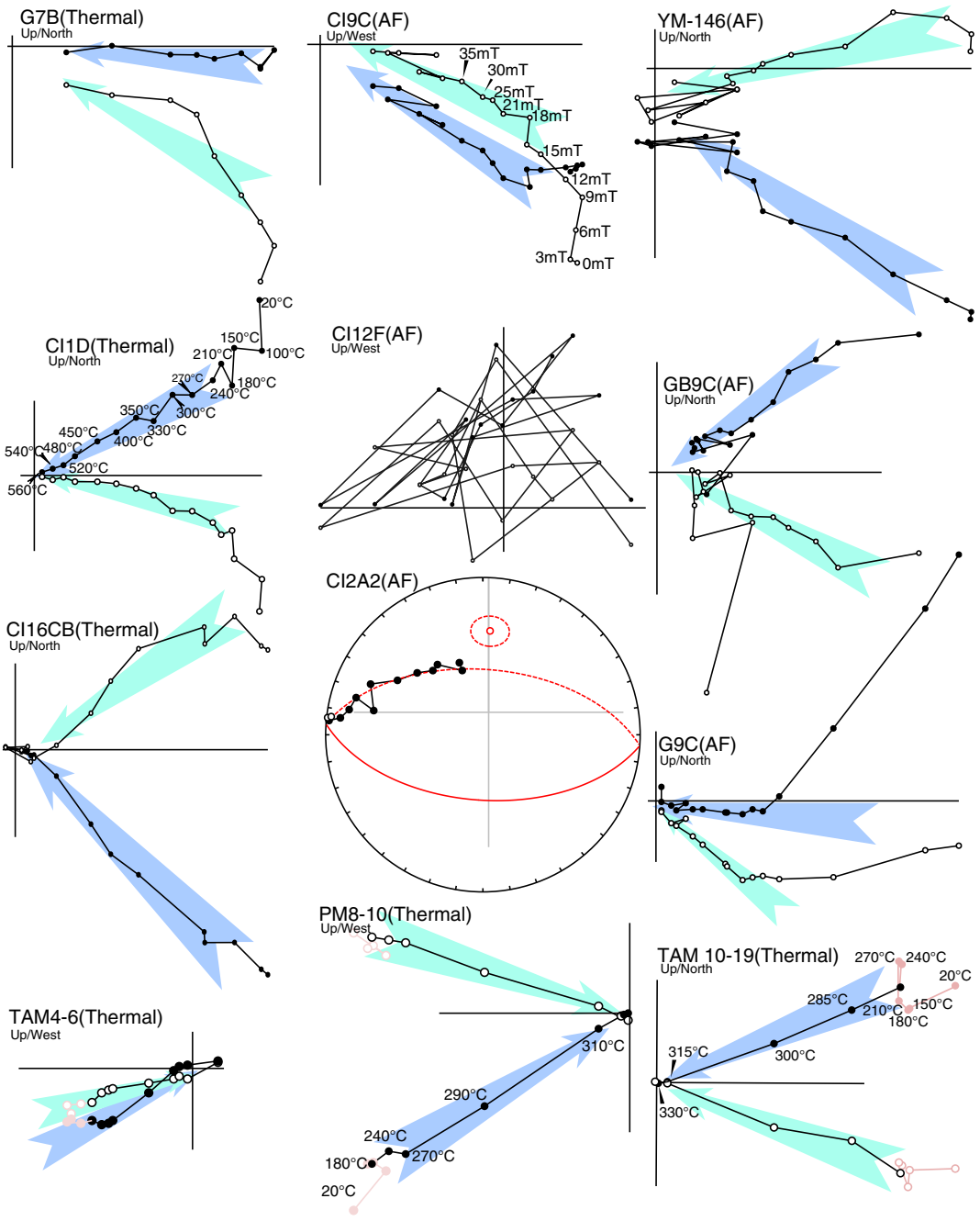

Fig. 3. Examples of Zijderveld diagrams. Solid (open) circles correspond to projection onto the horizontal (vertical) planes. Temperature and AF steps are the same for all samples as the noted in the examples. TAM and PM codes refer to Cambrian Limestones, published in Pastor-Galan et al. (2015a) and shown to simplify the read of the paper. All the remainder shows results from Carboniferous granitoids.

the other hand, NRM acquisition over a prolonged interval may also smear out short-duration PSV and then essentially represents a geocentric axial dipole direction. We applied a fixed 45° cut-off to the VGP distributions of each locality except for the Tamames limestone whose VGP distribution shows some remarkable features (see discussion).

4.2. Post-kinematic granitoids

We sampled 83 cores and three blocks, in eight plutonic bodies (Fig. 4; sample_locations.kml file in supplementary material), six of the bodies are known to be post-kinematic with U–Pb crystallization ages in zircons spanning from 310 to 300 Ma (Béjar [2 sites], Villavieja de Yeltes, Cipérez, La Alberca and El Álamo plutons; Gutiérrez-Alonso et al., 2011a). The age of the other two bodies is unknown, but they are interpreted to be post-kinematic because of their petrological similarities and vicinity to dated post-kinematic granitoids (Navarredonda de Gredos and San Martín del Pimpollar; Gutiérrez-Alonso et al., 2011a; Díaz Alvarado et al., 2013).

Many specimens appear to be too weakly magnetic to recover any meaningful Characteristic Remanent Component (ChRM hereafter, see supplementary material file demagnetization.zip). In 12 specimens we recovered a clear ChRM component (MAD < 15°) and in 39 specimens we could fit great circles that passed through the aforementioned component and a present day component (Fig. 4; Table 1). After combining

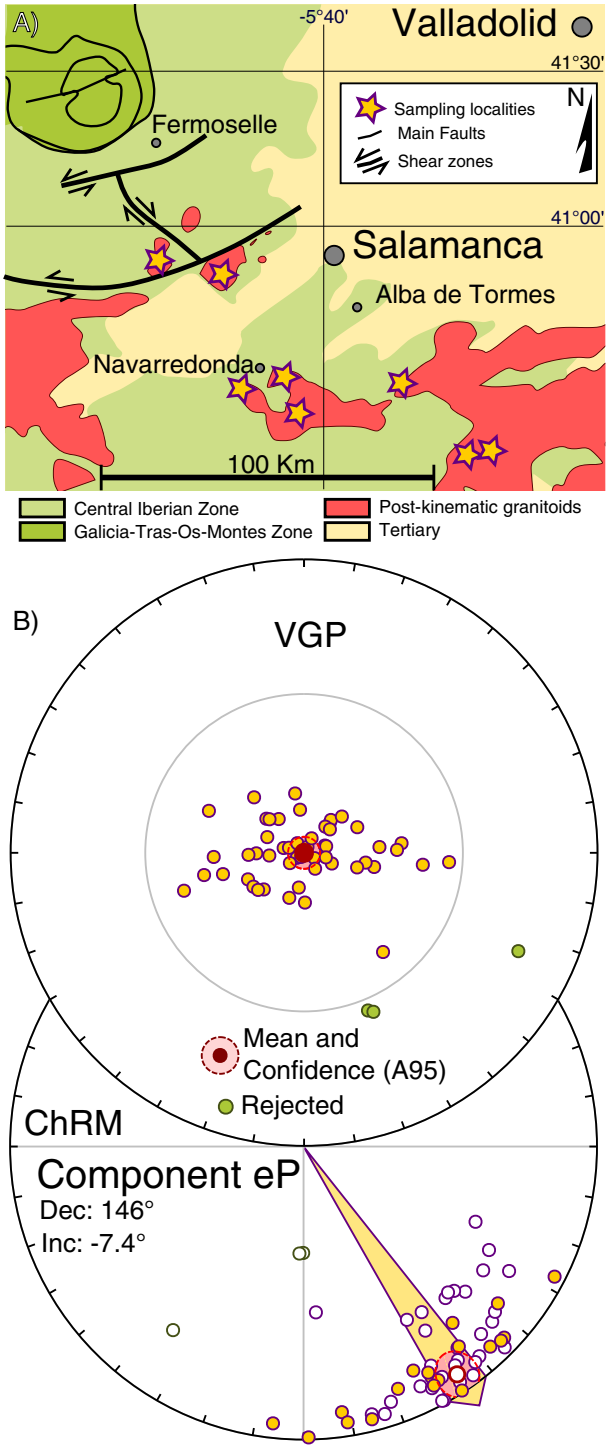

Fig. 4. A) Site locations in the post-kinematic granitoids. B) VGP and ChRM results and statistical parameters. Open circles in VGP are projections into the upper hemisphere.

great circle solutions and linear best fits (McFadden and McElhinny, 1988) we defined a ChRM for the post-kinematic rocks that we named eP because of its similarity to the eP magnetization component in the Cantabrian Zone (e.g. Weil et al., 2000). This eP component in our collection is of single polarity with declination/inclination = 146°/−7.4° (K = 21.3 and A_{95} = 4.4°). A_{95} lies between A_{95}max and A_{95}min (Table 1) although the VGP distribution is notably elongated (Fig. 5).

4.3. Syn-kinematic granites

We have sampled the syn-kinematic granites in two different extensional domes: the larger Tormes Dome (58 cores and 11 blocks), which surrounds the Morais Complex (Fig. 6) and the smaller Martinamor Dome (21 cores), located to the south of the Morais Complex, in the southern limb of the Central Iberian curve (Fig. 7).

4.3.1. Tormes Dome

We have identified three different components in the samples taken in the Tormes Dome (Table 1; Fig. 5). A low temperature component showing Dec/Inc = 5.1°/53.9° was identified in most (112) of the analyzed specimens (Fig. 5; Table 1; file demagnetization.zip in supplementary material). We consider this component as a Viscous Remanent Magnetization (VRM), because of similarity to the Quaternary Geocentric axial dipole (in Salamanca: Dec/Inc = 0/60°). We have also found reversed directions to this component (Fig. 5) in site G6 (file Tormes.dir in demagnetization.zip in the supplementary material). We interpret that site as remagnetized during a reversed chron in the Neogene.

In 35 of the specimens we identified a single polarity NRM component with Dec/Inc = 150.4°/−1.3° (K = 77.6 and A_{95} = 2.8°), i.e. with a similar attitude as that retrieved from the post-kinematic granitoids. We have grouped this component with the eP component of the post-kinematic granitoids since it passes the common true direction tests of McFadden and McElhinny (1990) and Tauxe et al. (2010; see supplementary material's Common_true_eP.pdf).

Finally, we have identified a component, labeled C, only found in the syn-kinematic granitoids that we consider the ChRM (Fig. 5; Table 1). This component was isolated in 53 specimens and additionally, we could fit 71 great circles that are a combination of the C component and either one of the previously described eP or present-day components (Fig. 5). The C component is dual-polarity that shares a common true mean direction (Fig. 6C). When combined (as reversed polarity), its direction is Dec./Inc. = 82.7°/15.4° (K = 15 and A_{95} = 3.4°, cf. Fig. 6 and Table 1).

4.3.2. Martinamor Dome

Contrary to the Tormes Dome, we only identified a single NRM component in the Martinamor Dome (Figs. 3, 4 and 7). Combining directions (13) and great circles (8) we obtained a dual-polarity component that shares a common true mean direction (Fig. 7C); Dec/Inc (reversed polarity) = 67.4°/11.4° (K = 12.6 and A_{95} = 10.1°; Fig. 7; Table 1). In addition, the reversed polarity shows a common true mean direction with both reversed and normal polarities of the C component of the Tormes Dome collection (see C-comp.pdf in the supplementary material). Therefore, we consider this to be the same C component in both domes.

5. Rock magnetism in the Tamames syncline

A total of 209 cores and 4 blocks were collected in three localities in the Tamames limestone Formation (Fig. 8A and C; sample_locations.kml file in supplementary material). Magnetic directions, demagnetization procedure and discussion of the results were reported in Pastor-Galan et al. (2015a). In this paper we provide extensive rock magnetic analyses to further evaluate the hypotheses casted in Pastor-Galan et al. (2015a, 2015b).

Identifying magnetic carriers provides crucial information about the magnetization, timing and information about the geological processes involved during the magnetization of the rock. We analyzed the anisotropy of magnetic susceptibility (AMS) and applied several rock magnetic analyses to the Cambrian limestones, including thermomagnetic experiments, hysteresis measurements and IRM component analysis (Kruiver et al., 2001), both a room temperature, with the goal of identifying the magnetic carrier(s).

Table 1
Statistics on the results per studied locality. N, number of successful analyses; Ns number of analyses passing the 45° cut-off; mDec, average declination; mInc, average inclination; k precision parameter on directions; α95, confidence cone at 95% on directions; K, precision parameter on poles; A95 confidence cone at 95% on poles. ΔDx and ΔIx confidence interval at 95% on declination and inclination.

	Component	Considering	N	Ns	mDec	mInc	R	k	α95	K	A95	A95min	A95max	ΔDx	ΔIx
Post-kinematic	eP	Only lines	12	12	149.3	2.5	11.1	11.8	13.2	14.5	11.8	4.4	17.1	11.8	23.6
		Lines + circles	51	59	146	−7.4	47.4	13.9	5.6	21.3	4.4	2.5	6.9	4.4	8.7
Syn-kinematic															
Tormes DOME	C	Only lines	53	56	81.6	22	47	8.7	7.1	12.3	5.8	2.5	6.7	5.9	10.4
		Lines + circles	125	127	82.7	15.4	112.7	10.1	4.2	15	3.4	1.7	3.9	3.4	6.4
	eP	Only lines	34	35	150.4	−1.3	33.4	51.3	3.5	77.6	2.8	2.9	8.9	2.8	5.6
	Present day	Only lines	86	112	6.8	51.8	82	21.2	3.4	19	3.6	2	5	4.3	3.9
Martinamor dome	C	Lines + circles	18	21	67.4	11.4	16	8.5	12.6	12.6	10.1	3.8	13.3	10.2	19.7
Tamames	ChRM	Lines	234	234	123.5	9.5	215.7	12.8	2.7	14.3	2.5	1.4	2.6	2.5	4.9
C component	All results		142	149	81.1	15	127.5	9.7	4	14.5	3.2	1.7	3.6	3.3	6.1
eP Component	All results		85	97	148.1	−3.6	80.6	19.2	3.6	29.8	2.9	2	5	2.9	5.7

5.1. Thermomagnetic analyses

Thirteen high-field thermomagnetic runs were measured in air with an in-house-built horizontal translation-type Curie balance with a sensitivity of approximately 5×10^{-9} Am^2 (Mullender et al., 1993). About 50–80 mg of powdered sample material from representative lithologies were placed into quartz glass sample holders and were held in place by quartz wool. Heating and cooling rates were 6 °C min^{-1} and 10 °C min^{-1} respectively. Stepwise thermomagnetic runs were carried out with intermittent cooling between successive heating steps. The successive heating and cooling segments were 150, 100, 250, 200, 400, 350, 520, 450, 620, 550, 700 and 20 °C, respectively.

Nearly all samples only showed a paramagnetic contribution (supplementary material Thermomagnetic_curves.zip). Just in one

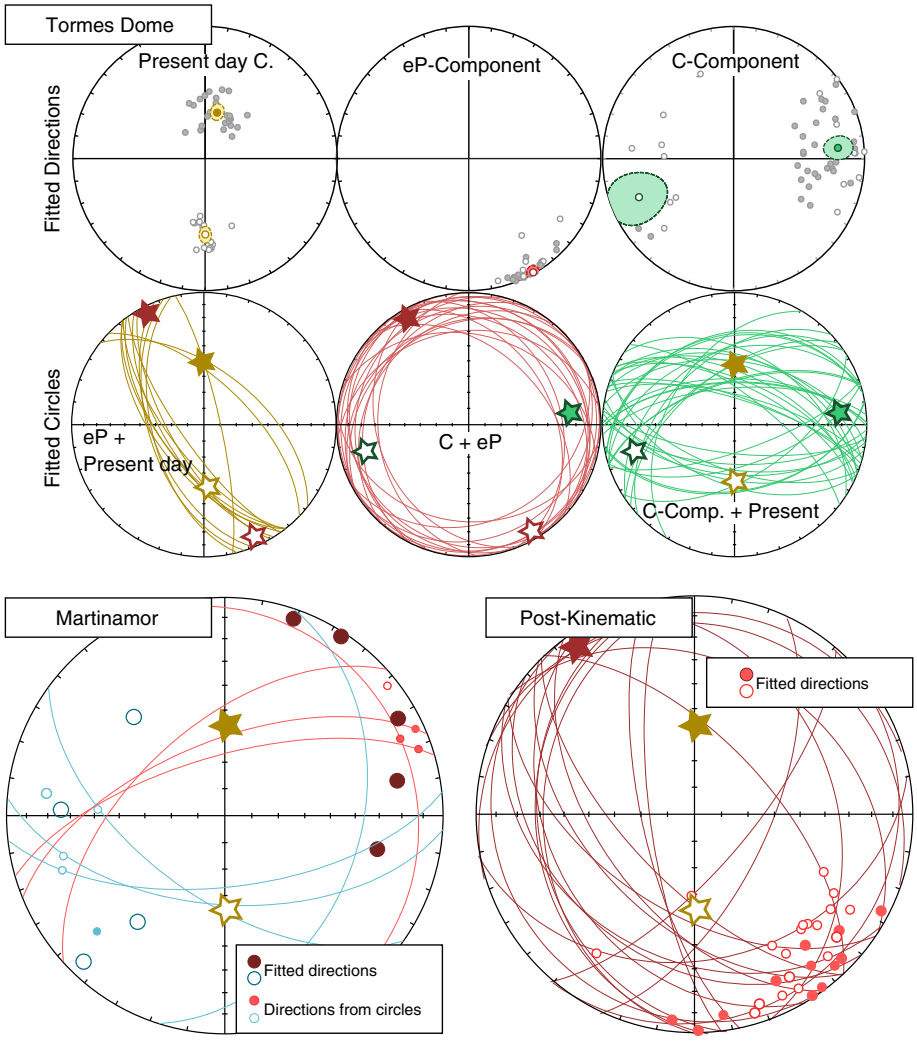

Fig. 5. Procedure to fit great circles. First we identified three components from linear vector end-point diagrams (Zijderveld, 1967): Present day, eP, and C. Once the components were established, we fitted great circles in those samples which did not yield distinguishable components. We selected only the circles that pass through two of the three identified components.

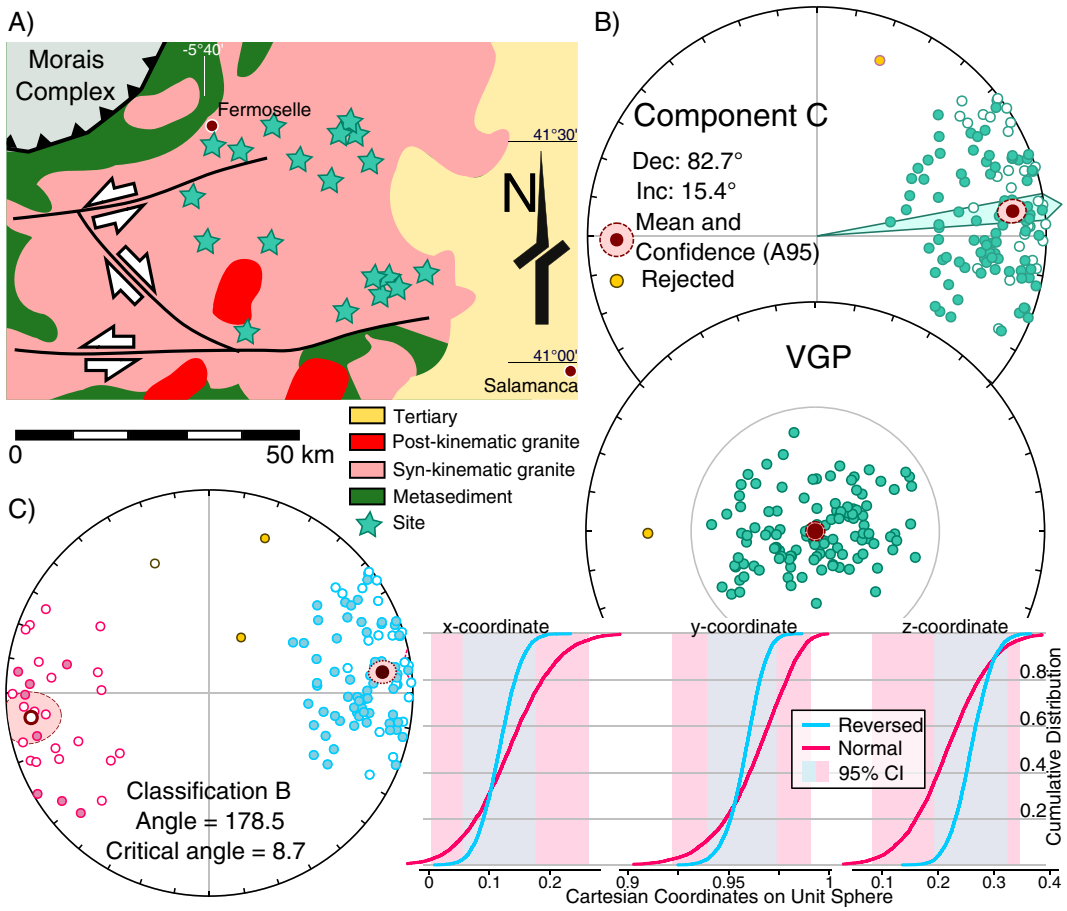

Fig. 6. A) Sites taken from the Tormes Dome. B) ChRM and VGP distributions with their statistical parameters. Open circles in VGP are projections into the upper hemisphere. C) Positive reversals test following methodologies of McFadden and McElhinny (1990) and Tauxe (2010). The McFadden and McElhinny (1990) test compares the two average directions (normal and reversed) and classifies the test as negative if they do not fit at a 95% confidence level. Additionally it classifies the positive tests depending on the critical angles, being A the best (low angles) and Indeterminate the worst (high angles). Our results show a classification of B (Critical angle = 8.7). The Tauxe (2010) method transforms a set of bootstrapped directions to cartesian coordinates [x, y, z]. Cumulative distributions of the Cartesian coordinates of the bootstrap are shown in panel C along with the bounds containing 95% of the means for each data set. All sets of directions are overlapping confirming that the two means cannot be distinguished at the 95% confidence level.

thermomagnetic run pyrrhotite could be identified, albeit dominantly the non-magnetic variety (hexagonal) (Fig. 9B). However, the presence of pyrrhotite also was inferred from the demagnetization diagrams from the ChRM component with a maximum unblocking temperature of ~320 °C (Fig. 9B) and the very high coercitivity in such ChRM (no demagnetization at 100 mT; Pastor-Galan et al., 2015a, 2015b). All pyrrhotite varieties are platy, monoclinic pyrrhotite (Fe_7S_8) has a Curie temperature of 325° (e.g. Dekkers, 1988). Pyrrhotite occurs commonly as a secondary mineral in high-diagenetic and very low-grade metamorphic limestones (Appel et al., 2012; Aubourg et al., 2012).

5.2. Hysteresis loops

We analyzed eleven hysteresis loops (at room temperature) with an alternating gradient force magnetometer (MicroMag Model 2900 with 2 Tesla magnet, Princeton Measurements Corporation, noise level 2×10^{-9} Am^2). Representative samples with masses ranging from 20 to 50 mg were measured using a P1 phenolic probe. Hysteresis loops were measured to determine the saturation magnetization (M_s), the saturation remanent magnetization (M_{rs}), and coercive force (B_c). These parameters were determined after correction for the paramagnetic contribution. The maximum applied field was 1 T. The field increment is 10 mT and the averaging time for each measurement was 0.15 s.

Different loop shapes were found (Fig. 9C; Hysteresis_raw.zip in supplementary material for all loops): (i) Wasp-waisted or goose-necked loops that do not saturate at 1 T which point to the presence either of two magnetic carriers or two particle-size distributions with distinct coercivity windows (TAM9-4P) indicating the presence of a hard (likely pyrrhotite) and a soft phase (either soft pyrrhotite or magnetite); (ii) pseudo-single domain loops (TAM1-9), that hardly saturates at 1 T indicating fine grained pyrrhotite; (iii) typical single domain (SD) loops (TAM3-8) likely indicating magnetite; (iv) very narrow loops suggesting quasi superparamagnetic behavior pointing to very fine-grained magnetic particles (TAM2-3-15), plausibly magnetite particles.

5.3. IRM acquisition curves

We have obtained 96 isothermal remanent magnetization (IRM) curves from our Tamames limestone samples covering the entire syncline. They were obtained with the robotized magnetometer system. Before the actual IRM acquisition, samples were AF demagnetized with the static 3-axis AF protocol with the final demagnetization axis parallel to the subsequent IRM acquisition field, a procedure that generates IRM acquisition curves with a shape as close to a cumulative-lognormal distribution as possible (Egli, 2004; Heslop et al., 2004). IRM acquisition curves consist of 61 IRM levels up to 700 mT.

5.3.1. IRM component analysis

IRM component analysis enables a semi-quantitative evaluation of different coercivity components (i.e. magnetic minerals) to a measured

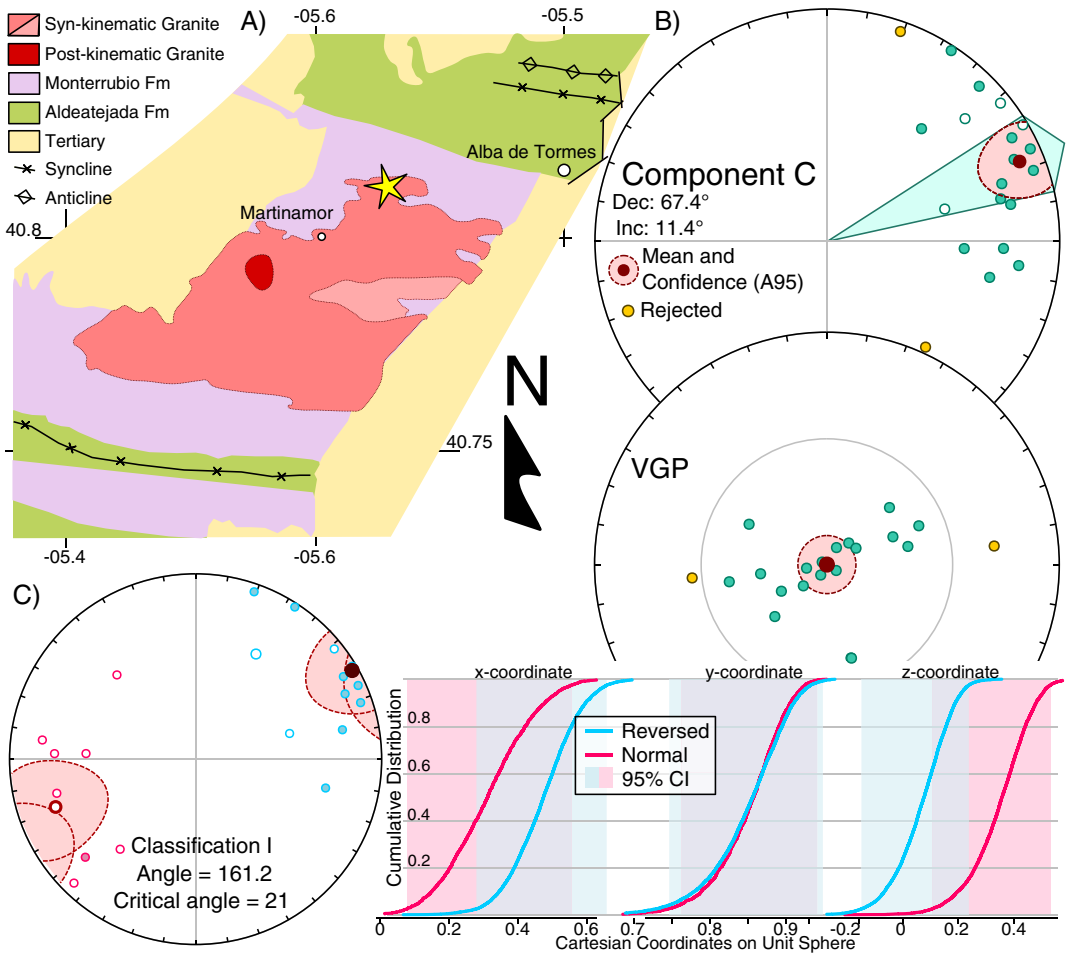

Fig. 7. A) Locality in the Martinamor Dome indicated by a yellow star B) ChRM and VGP distributions with their statistical parameters. Open circles in VGP are projections into the upper hemisphere. C) Positive reversals test, following methodologies of McFadden and McElhinny (1990) with classification I and Tauxe (2010), with 95% intervals of confidence overlapping in the three coordinates. (For interpretation of the references to color in this figure legend, the reader is referred to the web version of this article.)

IRM acquisition curve. 12 specimens were analyzed following the cumulative log-Gaussian approach (Kruiver et al., 2001). An example of fitted IRM acquisition is in supplementary material's file IRM_examples.pdf.

Measured IRM curves can be decomposed into one of more cumulative log-normal coercivity components representing individual magnetic mineral phases that are characterized by three parameters: (1) $B_{1/2}$, the field at which half of saturation isothermal remanent magnetization (SIRM) is reached; (2) M_{ri}, the magnitude of that phase, i.e. how much of it is present in the sample, providing an indication of the component's SIRM and therefore its contribution to the bulk IRM acquisition curve; and (3) DP: the dispersion parameter, expressing the width of the coercivity distribution of that mineral phase and corresponding to one standard deviation of the log-normal function (Kruiver et al., 2001; Heslop et al., 2002). Results from individual samples are characterized by two main IRM components: (a) a high coercitivity component with a high $B_{1/2} > 280$ mT and DP between 0.29 and 0.31 (log units); and (b) a second component 2 with $B_{1/2}$ ~45 mT and dispersion parameter (DP) of ~0.35 (log units). Component 1 is present in all samples; SIRM percentages vary from 75% to ~100%. Component 2 therefore represents 0% to a maximum of ~25% of the SIRM. We interpret component 1 with high coercivity, to be pyrrhotite and component 2 to represent very fine-grained magnetite.

5.3.2. End member modeling

In an attempt to further shed light on the magnetic mineralogy and recognizing different remagnetization episodes, we performed end-member modeling as in Gong et al. (2009a). The program (Heslop and Dillon, 2007) to interpret the IRM acquisition curves uses the algorithm developed by Weltje (1997). It assumes that the measured data can be represented by a linear mixture of a number of invariant constituent components, which are referred to as end-members. By least-squares minimization calculated normative compositions are optimized to the measured IRM acquisition curves, eliminating the need for prior knowledge of end-member properties (cf. Weltje, 1997). For further information about this technique in the framework of remagnetization see the review by Dekkers (2012).

End-member modeling is a helpful technique for identifying remagnetized and non-remagnetized sedimentary rocks independent of paleomagnetic field tests and directional information (Gong et al., 2009a; Van Hinsbergen et al., 2010; Meijers et al., 2011; Dekkers, 2012; Aben et al., 2014; Huang et al., 2015a, 2015b). We have applied this technique in order to find possible remagnetization 'pulses' (e.g. syn-folding and/or post-folding) in the Tamames syncline. A two end-member model with a high r^2 value of 0.91 (supplementary material's IRMEnd_member.zip) is our preferred model. The three end-member model with an r^2 value of 0.96 shows an even better fit and represents the break-in-slope in the curve of r^2 vs. number of end-members. However, the third end-member (End Member 2 in Fig. 10 (the program happens to number end members in a random manner, not paying attention to similarity in shape for example)) appears to be represented by only three samples (Fig. 10). In addition, End Members 1 and 2 show unusual IRM curve shapes. Therefore, it was not considered further.

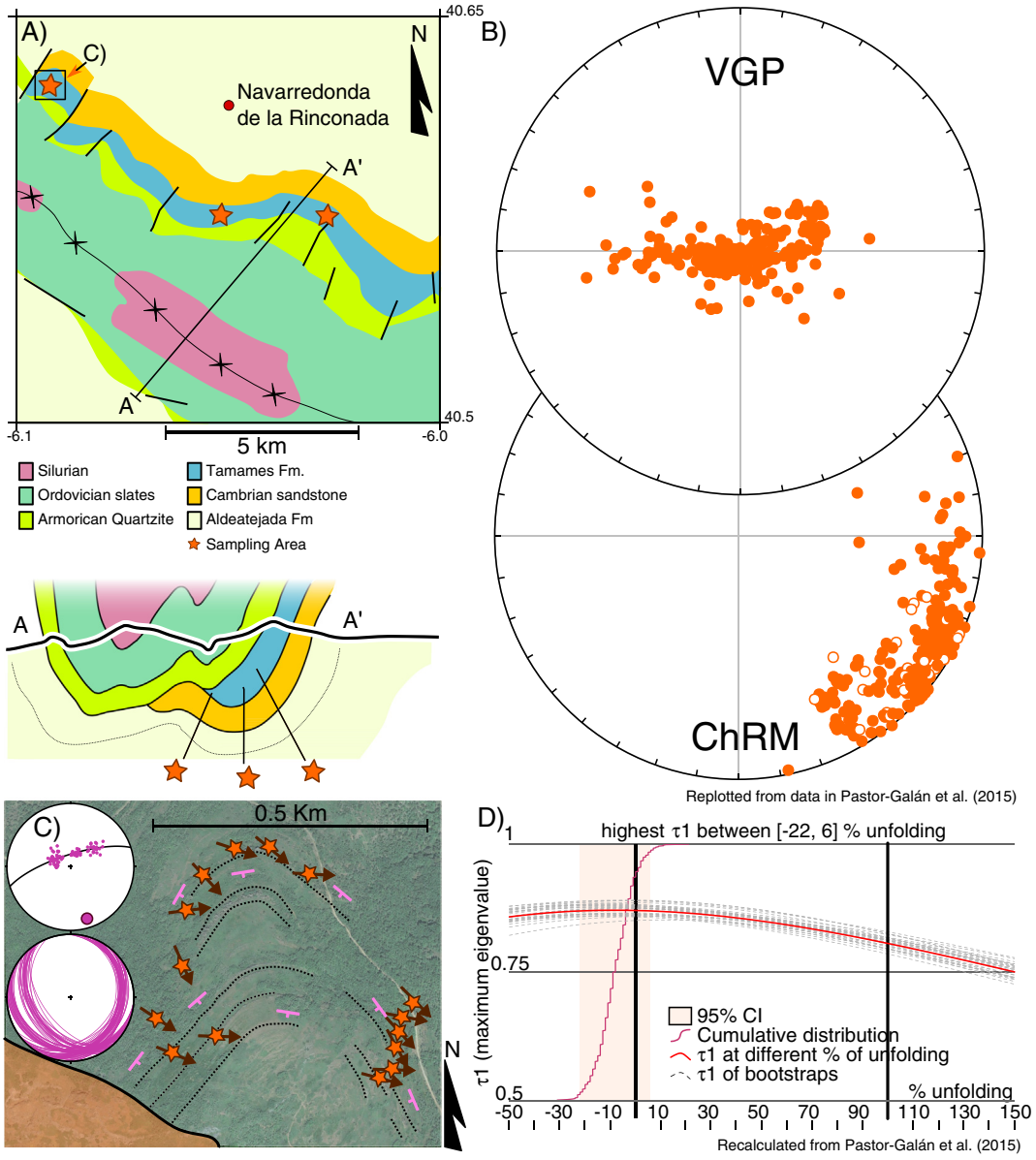

Fig. 8. A) Sampled localities in the Tamames Syncline both in map view and cross section. Note that both flanks of the syncline were sampled. B) ChRM and VGP distributions replotted Pastor-Galan et al. (2015a). C) Sites sampled in the "Las Peñas Albercanas" locality, just below the Cambro-Ordovician unconformity. Stereonets show π and β diagrams to calculate the fold axis at this locality. Arrows show approximate averages of the different sites. Note the absence of correlation between declinations and geographical and/or structural location. D) Negative fold-test for Tamames syncline. Data was corrected for the (tenuous) plunge of the fold.

To evaluate the coercivity distribution of the end members we applied IRM component analysis to these two end members (for the analysis of the three end member model see IRM_3End_member.zip in the supplementary material). The end members are characterized by two main IRM components: (a) a hard component 1 with a high $B_{1/2}$ of ~400 mT and DP ~0.30 (log units) which is the only component found in End Member 1; and (b) component 2 with $B_{1/2}$ ~30 mT and dispersion parameter (DP) of ~0.35 (log units) which occurs together with component 1 in End Member 2. In this end member, component 1 with large coercivity constitutes varying percentages of the SIRM from ~25 to ~100%; component 2 thus represents 0% to ~75% of the SIRM. We interpret component 1 (with high coercivity) to be pyrrhotite and component 2 to represent very fine-grained magnetite. These interpretations of the IRM component analysis are consistent with the other paleomagnetic and rock-magnetic experiments performed.

5.4. Anisotropy of the magnetic susceptibility

The majority of the NRM resides in pyrrhotite, in which the magnetic easy direction is confined to the basal crystallographic plane; the intrinsic anisotropy is very strong because of the 'hard' crystallographic c-axis (Schward and Vaughan, 1972; Schwarz, 1974). If pyrrhotite grows oriented in a preferred fabric, the magnetic remanence would be biased towards the fabric plane. As a corollary, AMS fabrics can reveal whether pyrrhotite would be oriented in a given geological fabric.

We measured the magnetic anisotropy of Tamames limestones to explore possible causes for the elongated VGP described here and in Pastor-Galan et al. (2015a). We determined the composite fabric of the paramagnetic, diamagnetic and ferromagnetic grains by measuring the anisotropy of magnetic susceptibility (AMS) of all 209 drilled samples from our Tamames syncline collection with an AGICO MFK1-FA susceptometer.

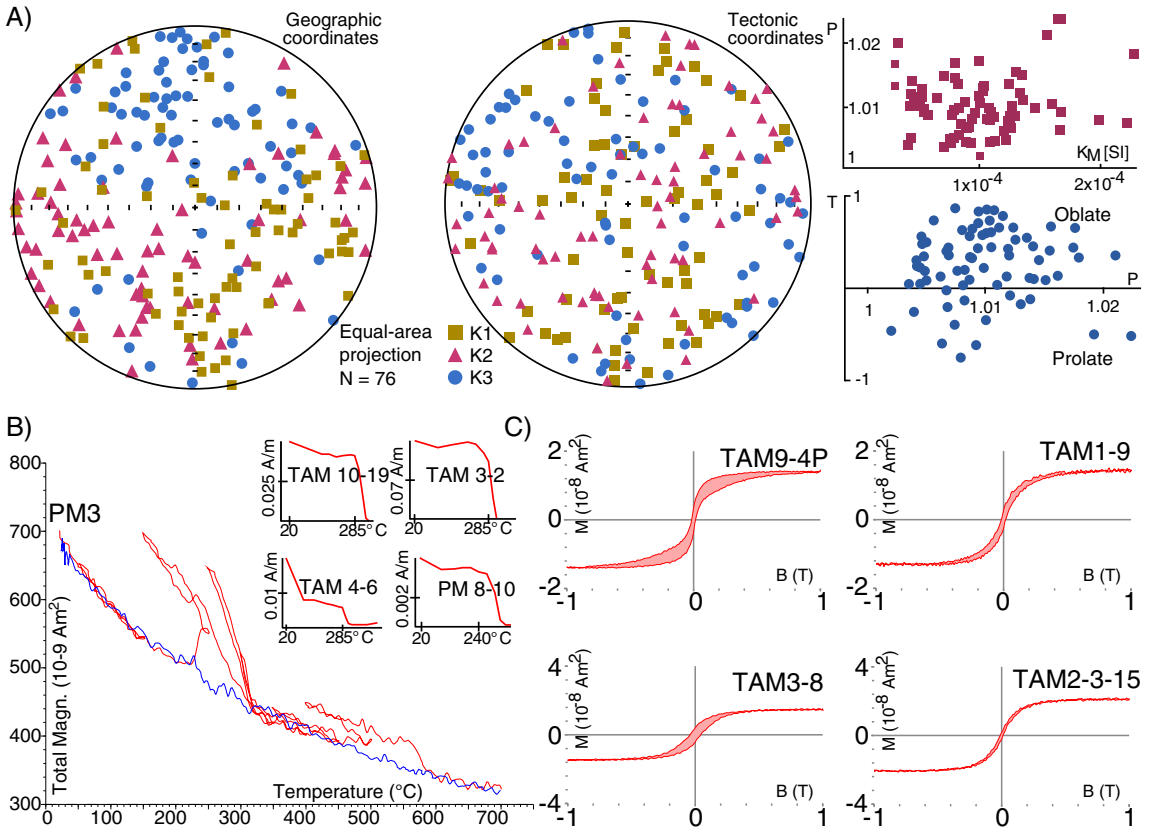

Fig. 9. AMS results for the Tamames limestones. Geographic coordinates seem to suggest a very weak N–S fabric. Tectonic coordinates appear to be random. B) Thermomagnetic curve of sample PM3 showing heating and cooling cycles, the only sample showing pyrrhotite. Accompanying in the right corner, four demagnetization curves of Tamames limestones, showing a sudden decay at 300–330 °C, which indicates pyrrhotite as dominant magnetic carrier. C) Four representative examples of hysteresis loops in the Tamames limestones: up-left, goose-necked loop; bottom left, single domain; up-right, pseudo-single domain; bottom right quasi-superparamagnetic loop (see text for details).

The degree of anisotropy (P) appears to be very low (<1.02; Fig. 9A) indicating a quasi-isotropic fabric at specimen level. The samples' three principal ellipsoid axes (Kmax, Kint, and Kmin) are distributed randomly both in geographic and tectonic coordinates (Fig. 9A). Actual measurements are in supplementary material (file AMS_raw.zip). The quasi-isotropic fabric precludes bias in NRM directions caused by a preferred orientation of pyrrhotite particles.

6. Discussion

The paleomagnetic sampling performed in the area surrounding the Morais Complex, together with previously published datasets (Pares and Van der Voo, 1992; Weil et al., 2013; Pastor-Galan et al., 2015a; Fernández-Lozano et al., 2016), permits the study of the kinematics of the Central Iberian curve during the Pennsylvanian (318 to 299 Ma). In the following sections we interpret the obtained results.

6.1. C component

We have assigned the C component in the Tormes and Martinamor domes (Figs. 6 and 7) as the ChRM. The average of the C component, in reversed polarity to ease comparison with the other results (see also Section 3), is Dec/Inc = 81.1°/15.0° (K = 14.5 and A_{95} = 3.2°; Fig. 11; Table 1). We interpret the C component as a primary magnetization acquired during the cooling of the syn-kynematic extensional granitoids. Three aspects support this interpretation: (1) the occurrence of normal and reversed polarities, (2) a low paleolatitude (λ) of 7.7°S (Table 1), and (3) a circular VGP distribution. The age of Tormes and Martinamor domes ranges between 325 to 318 Ma (Valverde-Vaquero et al., 2007; Costa et al., 2014; Gomes et al., 2014), just before and at the beginning of the reversed Kiaman superchron (e.g. Langereis et al., 2010). Therefore, the magnetization is likely to date from around the onset of the long-lasting Kiaman. We also know that Iberia crossed the Equator from the southern to northern hemisphere during the early Permian (Weil et al., 2010). A paleolatitude of 7.7°S constrains the pole to a youngest possible age of 318 Ma, and consequently as a primary (or pseudo-primary) magnetization. C components define a pole for the studied area of P_{lat}/P_{long} = 264°/−11.7° that we assigned to a minimum age of 318 Ma (Table 2). This pole shows the expected paleolatitude but also a counter-clockwise rotation exceeding 60° (Fig. 12) when compared to the global apparent polar wander path (GAPWaP) of Torsvik et al. (2012) calculated for Iberia (from Paleomagnetism.org, Koymans et al., 2016).

6.2. The Tamames syncline magnetization

Pastor-Galan et al. (2015a) described the Tamames ChRM as a single polarity (reversed) and with consistent shallow inclinations in in-situ coordinates (Average inclination = 9.5°). In contrast, the paleomagnetic declinations notably vary with orientations ranging from 78° to 169° (Fig. 8B; K = 20.2, A_{95} = 2.5°, cf. Table 1). The VGP distribution is very elongated, although A_{95} (2.5°) is between A_{95}min (1.4°) and A_{95}max (2.6°). Pastor-Galan et al. (2015a) interpreted the dispersion in declination and elongated VGP distribution (Fig. 8) as a remagnetization taking place during a counter-clockwise rotation related to the formation of the Cantabrian Orocline (315–297 Ma). We have performed extensive and new rock magnetic analysis to the same sample collection to test this rather unconventional interpretation of remagnetization over a prolonged time interval.

Following the results of the new rock magnetic analyses, pyrrhotite appears to be by far the dominant magnetic carrier. Pyrrhotite is a secondary mineral which is formed under anchimetamorphic and very

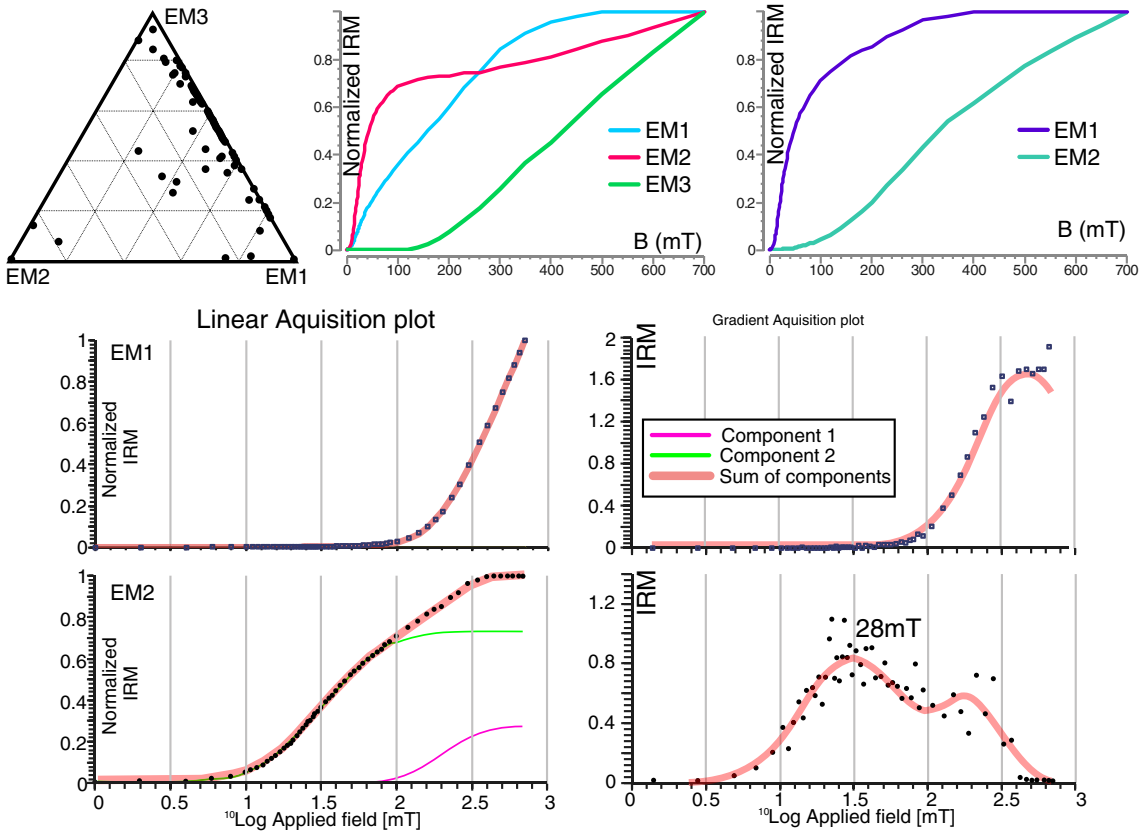

Fig. 10. IRM end member modeling results. At the top, results for 3 and 2 End Member models are shown. The ternary plot shows the percentages that each sample has from the three end-member model. Note that end-member 2 is represented mostly by three samples only with typical contributions of <10% in most other samples. We suggest that the entire sample variability can be robustly explained by two end members. Below, IRM component fitting of the end members in the 2 End Member model. Representative examples of the IRM component analysis. The components are marked with different lines: the linear acquisition plot (LAP) and the gradient acquisition plot (GAP) are shown in hatches. Component 1 has higher coercivity, Component 2 is relatively soft and is present only in end-member 2.

low grade metamorphic conditions (Aubourg et al., 2012). Some samples contain minor amounts of very fine grained magnetite, however all samples were totally demagnetized at 350 °C following the typical decay curves of pyrrhotite (Fig. 9; Dekkers, 1989). From the performed experiments we can deduce that magnetite in the Tamames limestones behaves as (quasi-)superparamagnetic, and therefore it does not carry an ancient remanence. Pyrrhotite is a strongly anisotropic mineral and within individual grains the magnetic easy direction is controlled by a strong basal plane anisotropy (Schward and Vaughan, 1972; Schwarz, 1974). It is, thus, relevant to test for pyrrhotite growth in a preferred stress field during metamorphism which could bias the obtained ChRM directions. The obtained AMS values show an almost isotropic fabric, incompatible with a preferred orientation of the pyrrhotite. So, the observed dispersion in declinations (Fig. 8B) represents the recording of the geomagnetic field, and not an artifact from a structural fabric.

We searched for possible correlations between the observed declinations and other parameters that could have influenced the NRM acquisition (distance between sites and granites and a contact metamorphism gradient, stratigraphic position, lithology, rock chemistry and IRM acquisition curves). There is no evidence of any kind of correlation between the declinations observed and the different parameters tested. For instance, we sampled several sites in a space of less than a square kilometer finding no relation between location and declination (Fig. 8C). Neither does declination correlate with the stratigraphic position, where declinations vary between strata with no particular order (Column.pdf in the supplementary material). IRM end member modeling could not reveal any kind of relation with any other geological constraint. Neither do IRM end-members correlate with declinations (i.e. a certain end member would dominantly show declinations of 80° and the other of 170°), geographic location, or stratigraphic position. For instance, samples TAM1-9 and TAM1-4 were collected less than two meters apart and show vastly different IRM end-member contributions. However, they show almost identical declinations (124° and 126°). In contrast, samples TAM10-16 and TAM10-19, separated a few centimeters, show very different declinations (152° and 85°) while having exactly the same IRM end-member contribution (20% and 80%) (supplementary material's IRMEnd_member.zip).

In contrast to the expected distribution in samples magnetized at low latitudes, here the distribution of the paleomagnetic directions shows a large scatter in declination and consistent inclinations. Additionally, the distribution in VGP is very elongated, suggesting an additional source of scatter to the magnetic field variations. The main candidates to produce such aberrant scatter in declination are: (i) structural complications, (ii) inclination shallowing, or (iii) vertical axis rotations.

Structural analysis of the Tamames syncline (π and β diagrams Fig. 8C) shows that Tamames Syncline is, at least locally, a simple structure: an open upright fold with a gently plunging fold axis (162°/15°). No major faults or other structures are found in the area (Fig. 8C). We can, therefore, discard structural complications as a source of scatter. The widespread presence of pyrrhotite, negative fold-test following the Tauxe and Watson (1994), and the fact that results gets sensibly more scattered after structural correction, implies that ChRM component is post-folding, and related to one or more remagnetization events. This result also discards inclination shallowing as a source of scatter. The only plausible cause, therefore, for the observed scatter is vertical axis rotations. Pastor-Galan et al. (2015a) calculated a reference declination of ~155° for Tamames based on the Early Permian pole obtained by Weil et al. (2010). Using the C component (~80°) and the reference direction,

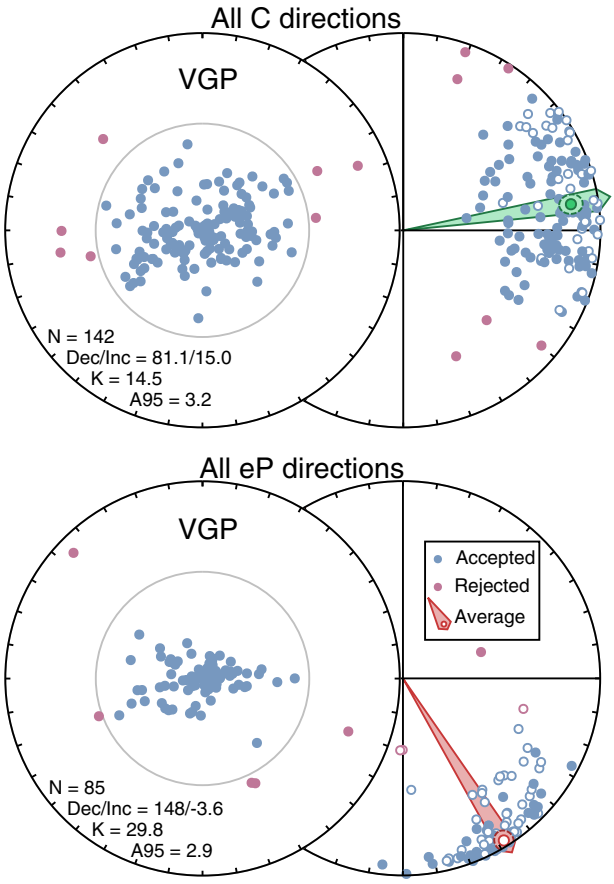

Fig. 11. Top, synthesis of C component combining results from the Tormes and Martinamor domes. Below, synthesis of eP component using directions from post-kinematic granitoids and the eP component from Tormes Dome. Both are showing average directions and their cones of 95% confidence and other statistical parameters. C component averages, A95 and parachute of ΔDeclination are in green and eP in red.

we find that the Tamames region rotated about 70° counter-clockwise, which fits in both magnitude and time (310–297 Ma) with the expected rotation if Tamames syncline is considered a part of the southern limb of the Cantabrian Orocline (Pastor-Galán et al., 2011; Weil et al., 2013; Pastor-Galan et al., 2015a). The Central Iberian curve hypothesis explicitly demands a clockwise rotation to accommodate the "S" shape around the Morais Complex (Fig. 1A).

It is challenging to explain how a small area as the Tamames syncline registrated a 10 Myr protracted process of remagnetization. Remagnetization during rotation is a non-unique process. Gong et al. (2009b) documented remagnetization during rotation locked into the rocks in various rather small basins during the middle Cretaceous rotation of Iberia. It is indeed true that these basins show a single remagnetization direction across an entire basin and not a rotation recorded in samples from a single basin (please, note that in Organyà Basin the recorded rotation is argued to be from non-remagnetized

Table 2
Pole for Iberia at 318 Ma and polar wander path obtained from the moving average (see text for details).

	Age (Ma)	Plong	Plat	A95
C-comp	318.0	264.0	−11.7	3.2
Movavg4	307.5	249.0	9.5	2.3
Movavg3	305.0	239.6	21.7	1.3
Movavg2	300.0	231.0	29.8	1.7
Movavg1	297.5	215.1	37.5	2.3
	Lat	41		
	Lon	−6		

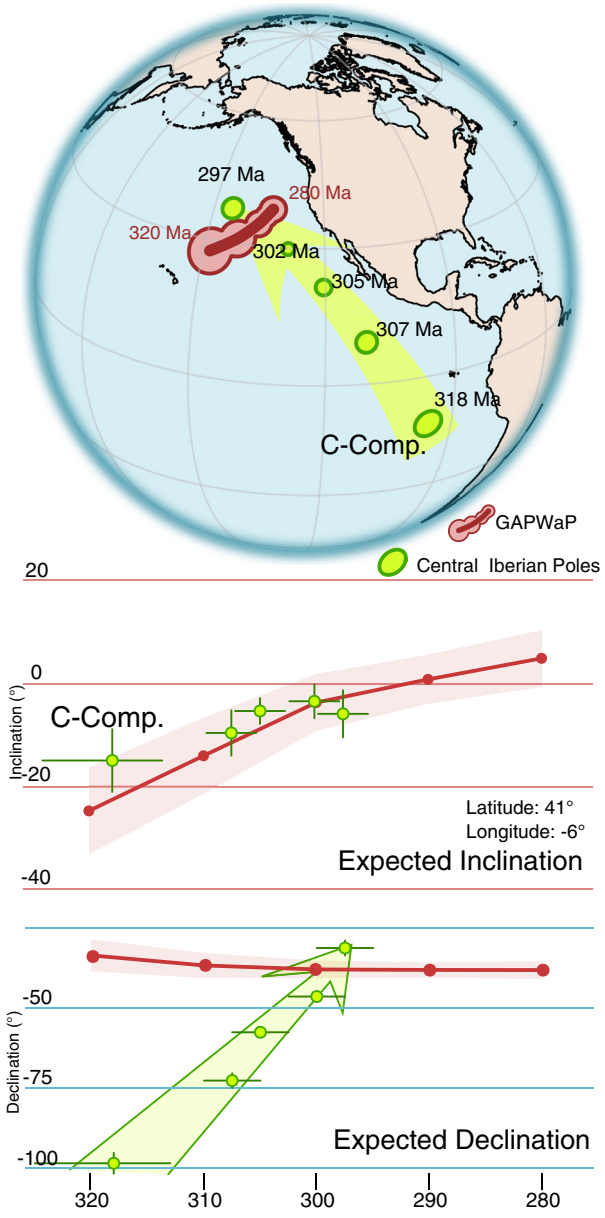

Fig. 12. Apparent polar wander path for Central Iberia (in green) compared to the GAPWaP (in red). The path consists on the C-component of this paper and a moving average for the Tamames and eP directions as described in the text (values in Table 2). The path shows a ca. 70° counter-clockwise rotation, consistent with Central Iberia being part of the Cantabrian orocline and discarding a secondary origin for the Central Iberian curve. (For interpretation of the references to color in this figure legend, the reader is referred to the web version of this article.)

rocks, cf. Gong et al., 2009a, 2009b). This absence of analog situations may make the process suggested here counter-intuitive. However, in our view it is the most plausible scenario to explain the paleomagnetic and rock magnetic results,. First, it is important to notice that the Tamames syncline outcrop is surrounded by post-kinematic granitoids (Fig. 2) of ages that span the period between 310 and 300 Ma (Gutiérrez-Alonso et al., 2011a).

We suggest that the NRM acquisition of the Tamames limestones happened as a consequence of a complex granitoid-induced fluid-plumbing system that took advantage of differences in porosity in the limestones, fractures, bedding, and possibly the angular unconformity below the lower Ordovician quartzites. Fluids, would have remagnetized the rock in a quasi-random style, following the lack of correlation between different magnetic properties and ChRM directions. The process would transform pyrite and magnetite into pyrrhotite. Pyrrhotite is

quite stable in low-grade rocks under reducing conditions, so the portions of the rock that got remagnetized with the first arrival of fluids would remain unaffected by the next pulses of fluids. A 'front of remagnetization' would affect the rock where fluid can migrate (fractures, differential porosity…). In the scenario, the fluid causes pyrrhotite formation but once formed pyrrhotite is either immune to further reaction and/or the rock is cemented precluding further fluid migration at that specific spot.

The process may be more common than we currently suspect it appears to be. Most of paleomagnetic applications to tectonics disregarded the meaning of elongated VPGs and have used site averages. A syncline like Tamames, would traditionally consist of a maximum of three or four site averages. Those mean directions would oversimplify the data, losing the crucial information about remagnetization during vertical axis rotation that the data contain.

6.3. eP component

All post-kinematic and some syn-kinematic granitoid samples yielded a single polarity component with declinations to the SE and very shallow inclinations. With such results, the magnetization had to be acquired during a reversed superchron, when Iberia was situated at equatorial latitudes. The data obtained constrain the eP component to Late Carboniferous–Early Permian times, being primary for the post-kinematic granitoids, and an overprint in the syn-kinematic granitoids. We have named this component eP due to its similarity with the eP component observed in the core of the Cantabrian Orocline (Weil et al., 2013). The average parameters of component eP are Dec/Inc = 148°/−3.6° (K = 29.8 and A_{95} = 2.9°; Table 1). Like in the Tamames syncline, this component is also characterized by an elongated VGP distribution (Fig. 11) with ~75° of variability in declination (from 120° to 195°) and very consistent shallow inclinations. A_{95} is in between A_{95}min and A_{95}max, meaning that the average of the data set can be considered representative. Contrary, for low latitudes is expected a larger scatter in inclination rather than declination (Deenen et al., 2011).

In line with the Tamames interpretation, we interpret the elongated VGP distribution (scatter in declination) is a consequence of NRM acquisition during the ca. 70° counter-clockwise rotation. Post-kinematic granitoids emplaced in the same interval as the Cantabrian Orocline formed (Gutiérrez-Alonso et al., 2011a, 2011b; Weil et al., 2013). There is, however, a difference between the declination directions from the Tamames syncline (80°–170°) and those of the eP component (120°–195°). We argue that this difference is caused by the timing of the NRM acquisition. Whereas Tamames syncline rocks remagnetized through pulses of fluids coming from the surrounding post-kinematic granitoids in a chemical process, the post-kinematic granitoids only acquired their NRM once they were cold enough, so delayed to variable extents with respect to the Tamames limestone. In that way, Tamames limestones would have recorded mostly the first stages of the rotation, approximately about two thirds of it (its average declination is ~124°, Table 1) and the post-kinematic granitoids (with average declination 148°) would record primarily the later stages, until completion.

6.4. Apparent polar wander path

Tamames limestones and the eP component cover all the possible declinations between the pole obtained in the syn-kinematic granites (Dec. = 80°) and the pole obtained for stable Iberia in the Early Permian (Dec. = 155°). Since the Tamames and eP components were likely acquired during the formation of the Cantabrian Orocline, we have constructed an apparent polar wander path for the studied area between 318 and 297 Ma (Fig. 12; Table 2). The first point of the path is the pole obtained from the syn-kinematic granitoids for 318 Ma. We have obtained the other four poles (Table 2) combining all individual directions from Tamames limestones and the eP component. The datapoints were ordered by declination, assuming that easterly declinations were acquired earlier, since their directions are closer to the syn-kinematic granitoid direction. Southerly declinations are considered to have been acquired subsequently, since they are similar to the Early Permian pole for stable Iberia (Weil et al., 2010). From this distribution, we obtained a moving average of 93 data-points and steps of 31, therefore each pole shares 31 data points with the neighboring poles. We assigned the ages (Table 2) assuming a constant rotation rate of the Cantabrian orocline from 310 to 297 Ma (Pastor-Galán et al., 2011; Weil et al., 2013). The resulting apparent polar wander path fits in paleolatitude with the GAPWaP (adapted for Iberia from Paleomagnetism.org; Torsvik et al., 2012; Koymans et al., 2016) but shows a continuous counterclockwise rotation following the remagnetization during rotation (Fig. 12).

6.5. Kinematic evolution of the Central Iberian curve: "two" many oroclines in Iberia

The Cantabrian and Central Iberian orogenic curves draw an "S" in plan-view throughout Iberia (Fig. 1). If this "S" geometry is the product of secondary oroclinal bending, declinations would contort around such a geometry resulting in clockwise rotations in the northernmost and southernmost limbs and counter-clockwise rotations in the then shared intermediate limb. It would be expected that strong changes in declination would take place around the hinges of both oroclines. This observation is true for the Cantabrian Orocline, its northern limb shows clockwise rotations (Weil et al., 2013; Edel et al., 2014, 2015; Pastor-Galán et al., 2015b), and around the hinge declinations progressively turn around until they indicate counter-clockwise rotation for the shared limb (southern limb of the Cantabrian Orocline; Weil et al., 2000, 2001; Fernández-Lozano et al., 2016). However, the results we have found around the hinge and southern limb of the putative Central Iberian orocline together with previous results from the literature (Perroud et al., 1991; Pares and Van der Voo, 1992; Pastor-Galan et al., 2015a) show consistent counter-clockwise rotations (Figs. 12 and 13). The latter rotations are in full agreement with the counter-clockwise rotations observed in the southern limb of the Cantabrian Orocline (Fig. 13; Weil et al., 2013; Pastor-Galan et al., 2015a). From the kinematic point of view, our results do not allow the formation of the Central Iberian curve after 318 Ma, in contrast to what was proposed by several authors (Martínez-Catalán, 2011; Shaw et al., 2012; Weil et al., 2013; Martinez Catalan et al., 2014; Shaw et al., 2014, 2016).

Our results can only be interpreted in the sense of permitting the Central Iberian curve to be an inherited feature that originated prior to the extensional collapse of the Variscan orogen which produced the syn-kinematic granitoids, if it ever existed. Therefore, the curved geometry may be either a syn- or pre-collisional feature. Examples of plausible mechanisms capable of producing large scale, hairpin-shape progressive oroclines (i.e. syn-collisional) are indentation of a sharp and large rigid block during earlier collision (e.g. in Late Devonian or Early Carboniferous times) or a roll-back of a subducting slab previous to the final continent-continent collision (e.g. Rosenbaum et al., 2012). Until now, there is no evidence for either of these processes. Another possibility is that the Central Iberian curve is an inherited primary feature (e.g. a large embayment). However, this hypothesis would require a particular distribution of sedimentary rock facies which is not observed in the Central Iberian Zone (Aramburu et al., 2002).

We coin that the Central Iberian curve is just a mislead observation. The putative hinge of the Central Iberian curve is largely covered, being the Galicia–Tras-os-Montes Zone and Morais Complexthe only place where its trace is observable (Figs. 1 and 2). The peculiar geometry of Morais has to be explained by other mechanisms rather than vertical axis rotations (Martinez Catalan et al., 2014) since neither a secondary nor a progressive orocline scenario satisfies the available paleomagnetic data. Up to now, there are two kinematic models that explain the curved geometry of Morais Complex that do not invoke large differential vertical axis rotations: (1) The allochtonous complexes are the relic of an extrusion wedge product of a non-cylindrical collision (Martínez-Catalán,

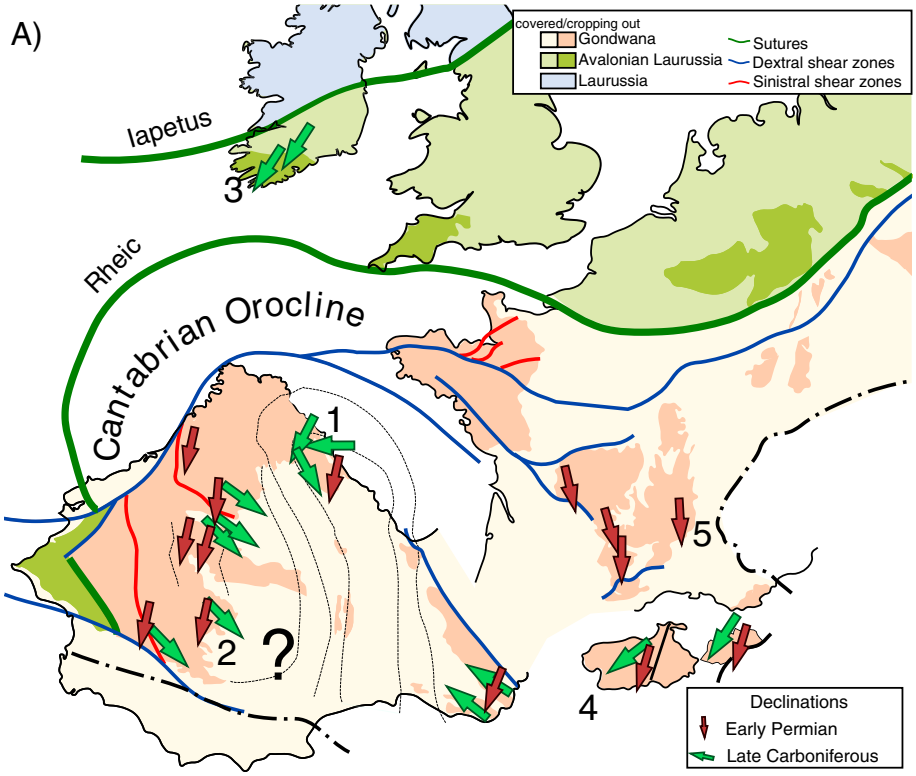

Fig. 13. Synthesis of paleomagnetic directions in Iberia, France and Ireland (see Weil et al., 2013 [1]; Pastor-Galan et al., 2015a [2] b [3]; Edel et al., 2014 [4] and 2015 [5]). Note the absence of Late Carboniferous clock-wise rotations around the Central Iberian curve.

1990; Frois da Silva, 2014); (2) Morais Complex is just a large scale rounded klippe of the larger allochthonous unit that thrusted over NW Iberia (Ries and Shackleton, 1971; Ribeiro, 1974). We find both explanations good starting hypotheses for further work to unravel the subtle nature of the Central Iberian curve.

7. Concluding remarks

Our new paleomagnetic data from intrusives from the Central Iberian Zone support 60° to 75° counter-clockwise rotations over its entire extension. This rotation is consistent in the Morais Complex region, where the alleged hinge of the Central Iberian curve was interpreted. The geometry of the Morais Complex can also be explained without invoking vertical-axis rotations: it could be a simple large scale klippe or an extrusion wedge. Our results are in agreement with the whole Central Iberian Zone being the southern limb of the Cantabrian Orocline, which starting from at least the Central Iberian Zone turns around NW Iberia and involves Southern Ireland and the Armorican Massif in France. From the kinematic point of view, our results do not permit the formation of the Central Iberian curve after 318 Ma, and therefore it is not a secondary orocline. No available paleomagnetic or geological data is in agreement with the Central Iberian curve to be a progressive orocline (e.g. indenter or roll-back) or a primary physiographic feature (e.g. a gulf, embayment). We conclude that the particular geometry of the Central Iberian Zone drove to kinematic misinterpretation in absence of reliable data. Therefore, the kinematic evolution of the Central Iberian curve requires revision.

Acknowledgments

We acknowledge the comments and suggestions by anonymous reviewer and editor that largely improved the paper. This research has been funded by ISES, The Netherlands. GGA is funded by the Ministry of Economy and Competitiveness under the project ODRE III-Oroclines & Delamination: Relations & Effects (CGL2013-46061-P) and the Founding Program for Research Groups by University of Salamanca. Funding for JFL comes from a contract under the Spanish Law of Science, established by the Junta de Castilla y León and the University of Salamanca.

This paper is a contribution to IUGS-UNESCO's IGCP projects no. 574 "Bending and Bent Orogens, and Continental Ribbons", no. 597 "Amalgamation and Breakup of Pangaea" and no. 648 "Supercontinent Cycles & Global Geodynamics".

Appendix A. Supplementary data

Supplementary data associated with this article can be found in the online version, at http://dx.doi.org/10.1016/j.gr.2016.06.016. These data include the Google map of the most important areas described in this article.

References

Aben, F.M., Dekkers, M.J., Bakker, R.R., van Hinsbergen, D.J.J., Zachariasse, W.J., Tate, G.W., McQuarrie, N., Harris, R., Duffy, B., 2014. Untangling inconsistent magnetic polarity records through an integrated rock magnetic analysis: a case study on Neogene sections in East Timor. Geochemistry, Geophysics, Geosystems 15, 2531–2554. http://dx.doi.org/10.1002/2014GC005294.

Aerden, D., 2004. Correlating deformation in Variscan NW-Iberia using porphyroblasts; implications for the Ibero–Armorican Arc. Journal of Structural Geology 26, 177–196.

Alcock, J.E., Martínez-Catalán, J.R., Arenas, R., Montes, A.D., 2009. Use of thermal modeling to assess the tectono-metamorphic history of the Lugo and Sanabria gneiss domes, Northwest Iberia. Bulletin de la Societe Geologique de France 180, 179–197.

Alcock, J.E., Martínez-Catalán, J.R., Pascual, F.J.R., Díez Montes, A., Díez Fernández, R., Gómez Barreiro, J., Arenas, R., Dias da Silva, I., González Clavijo, E., 2015. 2-D thermal modeling of HT–LP metamorphism in NW and Central Iberia: implications for Variscan magmatism, rheology of the lithosphere and orogenic evolution. Tectonophysics 657, 21–37.

Appel, E., Crouzet, C., Schill, E., 2012. Pyrrhotite remagnetizations in the Himalaya: a review. Geological Society, London, Special Publications 371, 163–180. http://dx.doi.org/10.1144/SP371.1.

Aramburu, C., Méndez-Bedia, I., Arbizu, M., 2002. The Lower Palaeozoic in the Cantabrian Zone (Cantabrian Mountains, NW Spain). In: García-López, S., Bastida, F. (Eds.), Cuadernos Del Museo Geominero, pp. 35–49.

Aubourg, C., Pozzi, J.-P., Kars, M., 2012. Burial, claystones remagnetization and some consequences for magnetostratigraphy. Geological Society, London, Special Publications 371, 181–188. http://dx.doi.org/10.1144/SP371.4.

Ballevre, M., Martinez Catalan, J.R., Lopez-Carmona, A., Pitra, P., Abati, J., Fernandez, R.D., Ducassou, C., Arenas, R., Bosse, V., Castineiras, P., Fernandez-Suarez, J., Gomez Barreiro, J., Paquette, J.-L., Peucat, J.-J., Poujol, M., Ruffet, G., Sanchez Martinez, S., 2014. Correlation of the nappe stack in the Ibero–Armorican arc across the Bay of Biscay: a joint French-Spanish project. Geological Society, London, Special Publications http://dx.doi.org/10.1144/SP405.13.

Bea, F., Montero, P., Zinger, T., 2003. The nature, origin, and thermal influence of the granite source layer of Central Iberia. The Journal of geology 111 (5), 579–595.

Bea, F., Montero, P., Gonzalez-Lodeiro, F., Talavera, C., Molina, J.F., Scarrow, J.H., Zinger, T., 2006. Zircon thermometry and U–Pb ion-microprobe dating of the gabbros and associated migmatites of the Variscan Toledo Anatectic Complex, Central Iberia. Journal of the Geological Society 163 (5), 847–855.

Capdevila, R., Floor, P., 1970. Les différents types de granites hercyniens et leur distribution dans le Nord-Ouest de l'Espagne. Boletín Geológico y Minero 81 (2–3), 215–225. Bea, F., Montero, P., Zinger, T., 2003. The nature, origin, and thermal influence of the granite source layer of Central Iberia. Journal of Geology 111 (5), 579–595.

Capdevila, R., Corretgé, L.G., Floor, P., 1973. Les granitoïdes de la Meseta Ibérique. Bulletin de la Societe Geologique de France XV (3–4), 209–228.

Castiñeiras, P., Villaseca, C., Barbero, L., Romera, C.M., 2008. SHRIMP U–Pb zircon dating of anatexis in high-grade migmatite complexes of Central Spain: implications in the Hercynian evolution of Central Iberia. International Journal of Earth Sciences 97, 35–50.

Castro, A., Corretgé, L.G., De la Rosa, J.D., Enrique, P., Martínez, F.J., Pascual, E., Lago, M., Arranz, E., Galé, C., Fernández, C., Donaire, T., López, S., 2002. Palaeozoic magmatism. In: Gibbons, W., Moreno, T. (Eds.), The Geology of Spain. Geol. Soc. (London), pp. 117–153.

Costa, M.M., Neiva, A.M.R., Azevedo, M.R., Corfu, F., 2014. Distinct sources for syntectonic Variscan granitoids: insights from the Aguiar da Beira region, Central Portugal. Lithos 196, 83–98.

Dallmeyer, R.D., Ibarguchi, J.I.G., 1990. Age of amphibolitic metamorphism in the ophiolitic unit of the Morais allocthon (Portugal) — implications for early Hercynian orogenesis in the Iberian Massif. Journal of the Geological Society of London 147, 873–878.

Dallmeyer, R.D., Martínez-Catalán, J.R., Arenas, R., Gil Ibarguchi, J.I., Gutiérrez-Alonso, G., Farias, P., Bastida, F., Aller, J., 1997. Diachronous Variscan tectonothermal activity in the NW Iberian Massif: evidence from $^{40}Ar/^{39}Ar$ dating of regional fabrics. Tectonophysics 277, 307–337. http://dx.doi.org/10.1016/S0040-1951(97)00035-8.

Deenen, M.H.L., Langereis, C.G., van Hinsbergen, D.J.J., Biggin, A.J., 2011. Geomagnetic secular variation and the statistics of palaeomagnetic directions. Geophysical Journal International 186, 509–520. http://dx.doi.org/10.1111/j.1365-246X.2011.05050.x.

Dekkers, M.J., 1988. Magnetic properties of natural pyrrhotite, part 1: behaviour of initial susceptibility and saturation-magnetization related rockmagnetic parameters in a grain-size dependent framework. Phys. Earth and Planet. Int. 52, 376–393.

Dekkers, M.J., 1989. Magnetic properties of natural pyrrhotite part II: high- and low-temperature behaviour of Jsr and TRM as function of grain-size. Physics of the Earth and Planetary Interiors 57, 266–283. http://dx.doi.org/10.1016/0031-9201(89)90116-7.

Dekkers, M.J., 2012. End-member modelling as an aid to diagnose remagnetization: a brief review. Geological Society, London, Special Publications 371, 253–269. http://dx.doi.org/10.1144/SP371.12.

Díaz Alvarado, J., Fernández, C., Castro, A., Moreno-Ventas, I., 2013. SHRIMP U–Pb zircon geochronology and thermal modeling of multilayer granitoid intrusions: implications for the building and thermal evolution of the Central System batholith, Iberian Massif, Spain. Lithos 175, 104–123.

Díez Balda, M.A., 1981. La estructura herciniana entre Salamanca y Sequeros (zona centro-ibérica). Cuadernos de geología Ibérica. Journal of Iberian Geology: an international publication of earth sciences 7, 519–534.

Díez Balda, M.A., 1986. El complejo Esquisto-grauváquico, las series paleozoicas y la estructura hercínica al Sur de Salamanca. Acta Salmanticensia, Sección de Ciencias, Universidad de Salamanca 52, 1–162.

Díez Balda, M.A., Vegas, R., González Lodeiro, F., 1990. Structure of the Central Iberian Zone. In: Dallmeyer, R.D., Martí¡nez García, E. (Eds.), Pre-Mesozoic Geology of Iberia. Springer, Berlin, pp. 172–188.

Díez Balda, M.A., Martínez-Catalán, J.R., Ayarza Arribas, P., 1995. Syn-collisional extensional collapse parallel to the orogenic trend in a domain of steep tectonics: the Salamanca Detachment Zone (Central Iberian Zone, Spain). Journal of Structural Geology 17, 163–182.

Domeier, M., Torsvik, T.H., 2014. Plate tectonics in the late Paleozoic. Geoscience Frontiers 5, 303–350. http://dx.doi.org/10.1016/j.gsf.2014.01.002.

Du Toit, A.L., 1937. Our Wandering Continents: An Hypothesis of Continental Drifting: "Africa Forms the Key". Oliver and Boyd (366pp.).

Edel, J.B., Schulmann, K., Holub, F.V., 2003. Anticlockwise and clockwise rotations of the Eastern Variscides accommodated by dextral lithospheric wrenching: palaeomagnetic and structural evidence. Journal of the Geological Society of London 160, 209–218. http://dx.doi.org/10.1144/0016-764902-035.

Edel, J.-B., Casini, L., Oggiano, G., Rossi, P., Schulmann, K., 2014. Early Permian 90 clockwise rotation of the Maures–Esterel–Corsica–Sardinia block confirmed by new palaeomagnetic data and followed by a Triassic 60 clockwise rotation. Geological Society, London, Special Publications http://dx.doi.org/10.1144/SP405.10.

Edel, J.-B., Schulmann, K., Lexa, O., Diraison, M., Géraud, Y., 2015. Permian clockwise rotations of the Ebro and Corso-Sardinian blocks during Iberian–Armorican oroclinal bending: preliminary paleomagnetic data from the Catalan Coastal Range (NE Spain). Tectonophysics 657, 172–186. http://dx.doi.org/10.1016/j.tecto.2015.07.002.

Egli, R., 2004. Characterization of individual rock magnetic components by analysis of remanence curves. Physics and Chemistry of the Earth Parts A/B/C 29, 851–867. http://dx.doi.org/10.1016/j.pce.2004.04.001.

Escuder Viruete, J., 1998. Relationships between structural units in the Tormes gneiss dome (NW Iberian massif, Spain): geometry, structure and kinematics of contractional and extensional Variscan deformation. Geologische Rundschau 87 (2), 165–179.

Escuder Viruete, J., Arenas, R., Martínez-Catalán, J.R., 1994. Tectonothermal evolution associated with Variscan crustal extension in the Tormes gneiss dome (NW Salamanca, Iberian Massif, Spain). Tectonophysics 238 (1), 117–138.

Escuder Viruete, J., Indares, A., Arenas, R., 1997. P–T path determinations in the Tormes Gneissic Dome, NW Iberian Massif, Spain. Journal of Metamorphic Geology 15, 645–663.

Fernández-Lozano, Pastor-Galán, D., Gutiérrez-Alonso, G., Franco, M.P., 2016. New kinematic constraints on the Cantabrian orocline: a paleomagnetic study from the Peñalba and Truchas Synclines, NW Spain. Tectonophysics (in press).

Fernández-Suárez, J., Gutiérrez-Alonso, G.G., Jeffries, T.E., 2002. The importance of along-margin terrane transport in northern Gondwana: insights from detrital zircon parentage in Neoproterozoic rocks from Iberia and Brittany. Earth and Planetary Science Letters 204 (1), 75–88.

Ferreira, N., Castro, P., Pereira, E., Dias, G., Miranda, A., 2000. Syn-tectonic plutonism and Variscan anatexis of a Cadomian crust (Miranda do Douro region). In: Dias, G., Noronha, F., Ferreira, N. (Eds.), Variscan Plutonism in the Central Iberian Zone (Northern Portugal). Eurogranites 2000, Guide Book (2000), pp. 155–172.

Franke, W., 1989. Variscan plate tectonics in Central Europe—current ideas and open questions. Tectonophysics 169, 221–228. http://dx.doi.org/10.1016/0040-1951(89)90088-7.

Frois da Silva, I., 2014. Geología de las zonas Centro Ibérica y Galicia – Trás-Os-Montes en la parte oriental del Complejo de Morais, Portugal/España, Serie Nova. Laboratiorio Xeoloxico de Laxe, A Coruña (428p.).

Gallastegui, G., 2005. Petrología del macizo granodiorítico de Bayo-Vigo (Provincia de Pontevedra, España). Serie NOVA TERRA n° 26. Área de Xeoloxía e Minería do Seminario de Estudos Galegos. Ediciós O Castro. Laboratorio Xeolóxico de Laxe (414 pp.).

Gomes, M.E.P., Teixeira, R.J.S., Neiva, A.M.R., Corfu, F., 2014. Geoquímica e geocronologia dos granitóides da região de Bemposta-Picote, Nordeste de Portugal. Comunicações Geológicas 101 (Especial I), 115–118.

Gómez Barreiro, J., Wijbrans, J.R., Castiñeiras, P., Mártinez Catalán, J.R., Arenas, R., García, F.D., Abati, J., 2006. $^{40}Ar/^{39}Ar$ laserprobe dating of mylonitic fabrics in a polyorogenic terrane of NW Iberia. Journal of the Geological Society 163 (1), 61–73.

Gong, Z., Dekkers, M.J., Heslop, D., Mullender, T.A.T., 2009a. End-member modelling of isothermal remanent magnetization (IRM) acquisition curves: a novel approach to diagnose remagnetization. Geophysical Journal International 178, 693–701. http://dx.doi.org/10.1111/j.1365-246X.2009.04220.x.

Gong, Z., van Hinsbergen, D.J.J., Dekkers, M.J., 2009b. Diachronous pervasive remagnetization in northern Iberian basins during Cretaceous rotation and extension. Earth and Planetary Science Letters 284 (3–4), 292–301.

Gutiérrez-Alonso, G., Fernández-Suárez, J., Weil, A.B., 2004. Orocline triggered lithospheric delamination. In: Weil, A.B., Sussman, A. (Eds.), Special Paper. Geological Society of America, Boulder, pp. 121–131.

Gutiérrez-Alonso, G., Murphy, J.B., Fernández-Suárez, J., Hamilton, M.A., 2008. Rifting along the northern Gondwana margin and the evolution of the Rheic Ocean: a Devonian age for the El Castillo volcanic rocks (Salamanca, Central Iberian Zone). Tectonophysics 461, 157–165. http://dx.doi.org/10.1016/j.tecto.2008.01.013.

Gutiérrez-Alonso, G., Fernández-Suárez, J., Jeffries, T.E., Johnston, S.T., Pastor-Galán, D., Murphy, J.B., Franco, M.P., Gonzalo, J.C., 2011a. Diachronous post-orogenic magmatism within a developing orocline in Iberia, European Variscides. Tectonics 30 (17 PP. doi:201110.1029/2010TC002845).

Gutiérrez-Alonso, G., Murphy, J.B., Fernández-Suárez, J., Weil, A.B., Franco, M.P., Gonzalo, J.C., 2011b. Lithospheric delamination in the core of Pangea: Sm–Nd insights from the Iberian mantle. Geology 39, 155–158. http://dx.doi.org/10.1130/G31468.1.

Gutiérrez-Alonso, G., Johnston, S.T., Weil, A.B., Pastor-Galán, D., Fernández-Suárez, J., 2012. Buckling an orogen: the Cantabrian Orocline. GSA Today 22, 4–9.

Gutiérrez-Alonso, G., Collins, A.S., Fernández-Suárez, J., Pastor-Galán, D., González-Clavijo, E., Jourdan, F., Weil, A.B., Johnston, S.T., 2015. Dating of lithospheric buckling: $^{40}Ar/^{39}Ar$ ages of syn-orocline strike-slip shear zones in northwestern Iberia. Tectonophysics http://dx.doi.org/10.1016/j.tecto.2014.12.009.

Heslop, D., Dillon, M., 2007. Unmixing magnetic remanence curves without a priori knowledge. Geophysical Journal International 170, 556–566. http://dx.doi.org/10.1111/j.1365-246X.2007.03432.x.

Heslop, D., Dekkers, M.J., Kruiver, P.P., Van Oorschot, I.H.M., 2002. Analysis of isothermal remanent magnetization acquisition curves using the expectation–maximization algorithm. Geophysical Journal International 148, 58–64. http://dx.doi.org/10.1046/j.0956-540x.2001.01558.x.

Heslop, D., McIntosh, G., Dekkers, M.J., 2004. Using time- and temperature-dependent Preisach models to investigate the limitations of modelling isothermal remanent magnetization acquisition curves with cumulative log Gaussian functions. Geophysical Journal International 157, 55–63. http://dx.doi.org/10.1111/j.1365-246X.2004.02155.x.

Holmes, A., 1929. A review of the continental drift hypothesis. Mining Publications 1–15.

Huang, W., Dupont-Nivet, G., Lippert, P.C., van Hinsbergen, D.J.J., Dekkers, M.J., Guo, Z., Waldrip, R., Li, X., Zhang, X., Liu, D., Kapp, P., 2015a. Can a primary remanence be retrieved from partially remagnetized Eocence volcanic rocks in the Nanmulin Basin (southern Tibet) to date the India–Asia collision? Journal of Geophysical Research - Solid Earth 120, 42–66. http://dx.doi.org/10.1002/2014JB011599.

Huang, W., van Hinsbergen, D.J.J., Dekkers, M.J., Garzanti, E., Dupont-Nivet, G., Lippert, P.C., Li, X., Maffione, M., Langereis, C.G., Hu, X., Guo, Z., Kapp, P., 2015b. Paleolatitudes

of the Tibetan Himalaya from primary and secondary magnetizations of Jurassic to Lower Cretaceous sedimentary rocks. Geochemistry, Geophysics, Geosystems 16, 77–100. http://dx.doi.org/10.1002/2014GC005624.
Johnston, S.T., 2001. The Great Alaskan Terrane Wreck: reconciliation of paleomagnetic and geological data in the northern Cordillera. Earth and Planetary Science Letters 193 (3), 259–272.
Johnston, S.T., Weil, A.B., Gutierrez-Alonso, G., 2013. Oroclines: thick and thin. Geological Society of America Bulletin 125, 643–663. http://dx.doi.org/10.1130/B30765.1.
Kirschvink, J.L., 1980. The least-squares line and plane and the analysis of palaeomagnetic data. Geophysical Journal International 62, 699–718. http://dx.doi.org/10.1111/j.1365-246X.1980.tb02601.x.
Kollmeier, J.M., van der Pluijm, B.A., Van der Voo, R., 2000. Analysis of Variscan dynamics; early bending of the Cantabria–Asturias Arc, northern spain. Earth and Planetary Science Letters 181, 203–216.
Koymans, M.R., Langereis, C.G., Pastor-Galan, D., van Hinsbergen, D.J.J., 2016. Paleomagnetism.org: an online multi-platform open source environment for paleomagnetic data analysis. Computers and Geosciences (in press).
Kruiver, P.P., Dekkers, M.J., Heslop, D., 2001. Quantification of magnetic coercivity components by the analysis of acquisition curves of isothermal remanent magnetisation. Earth and Planetary Science Letters 189, 269–276. http://dx.doi.org/10.1016/S0012-821X(01)00367-3.
Langereis, C.G., Krijgsman, W., Muttoni, G., Menning, M., 2010. Magnetostratigraphy — concepts, definitions, and applications. Newsletters on Stratigraphy 43, 207–233. http://dx.doi.org/10.1127/0078-0421/2010/0043-0207.
López-Carmona, A., Abati, J., Pitra, P., Lee, J.K.W., 2014. Retrogressed lawsonite blueschists from the NW Iberian Massif: P–T–t constraints from thermodynamic modelling and $^{40}Ar/^{39}Ar$ geochronology. Contributions to Mineralogy and Petrology 167, 987. http://dx.doi.org/10.1007/s00410-014-0987-5.
López-Moro, F.J., López-Plaza, M., Romer, R.L., 2012. Generation and emplacement of shear-related highly mobile crustal melts: the synkinematic leucogranites from the Variscan Tormes Dome, Western Spain. International Journal of Earth Sciences 101 (5), 1273–1298.
López-Plaza, M., 1982. Contribución al conocimiento de la dinámica de los cuerpos graníticos dela penillanura salmantino-zamorana (PhD Thesis) Universidad de Salamanca, Spain.
López-Plaza, M., Gonzalo, J., 1993. Caracterización geoquímica de las anatexitas del Domo del Tormes (provincias de Salamanca y Zamora). Revista de la Sociedad Geológica de España 6, 3–4.
López-Plaza, M., López Moro, F.J., Gonzalo Corral, J.C., Carnicero, A., 1999. Asociaciones de rocas plutonicas básicas e intermedias de afinidad calcoalcalina y shoshonítica y granitoides relacionados en el Domo Hercínico del Tormes (Salamanca y Zamora). Boletín de la Sociedad Española de Mineralogía 22, 211–234.
López-Plaza, M., López-Moro, F.J., Vicente-Tavera, A., Vicente-Villardón, J.L., 2008. Los leucogranitos equigranulares del Domo del Tormes (Zona Centro Ibérica): discriminación geoquímica mediante Biplot Canónico y significado petrogenético. E-Terra 5 (http://e-terra.geopor.pt/eng/index_en1.html).
Lotze, F., 1945. Zur gliederung der Variszichen der Iberischen Meseta. Geotektonísche Forschungen 6, 78–92.
Martínez, F.J., 1977. Données sur le métamorphisme regional hercynien dans le dome du Tormes. Geologische Rundschau 66, 91–98.
Martinez Catalan, J.R., Rubio Pascual, F.J., Diez Montes, A., Diez Fernandez, R., Gomez Barreiro, J., Dias da Silva, I., Gonzalez Clavijo, E., Ayarza, P., Alcock, J.E., Montes, A.D., Fernandez, R.D., Barreiro, J.G., Frois da Silva, I., Clavijo, E.G., Ayarza, P., Alcock, J.E., 2014. The late Variscan HT/LP metamorphic event in NW and Central Iberia: relationships to crustal thickening, extension, orocline development and crustal evolution. Geological Society, London, Special Publications 405, 225–247. http://dx.doi.org/10.1144/SP405.1.
Martínez, F.J., Julivert, M., Sebastian, A., Arboleya, M.L., Ibarguchi, J.G., 1988. Structural and thermal evolution of high-grade areas in the northwestern parts of the Iberian Massif. American Journal of Science 288 (10), 969–996.
Martínez-Catalán, J.R., 1990. A non-cylindrical model for the northwest Iberian allochthonous terranes and their equivalents in the Hercynian belt of Western Europe. Tectonophysics 179, 253–272.
Martínez-Catalán, J.R., 2011. Are the oroclines of the Variscan belt related to late Variscan strike-slip tectonics? Terra Nova 23, 241–247. http://dx.doi.org/10.1111/j.1365-3121.2011.01005.x.
Martínez-Catalán, J.R., 2012. The Central Iberian arc, an orocline centered in the Iberian Massif and some implications for the Variscan belt. International Journal of Earth Sciences 101, 1–16. http://dx.doi.org/10.1007/s00531-011-0715-6.
Martínez-Catalán, J.R., Arenas, R., García, F.D., Cuadra, P.G., Gómez-Barreiro, J., Abati, J., Castiñeiras, P., Fernández-Suárez, J., Martínez, S.S., Andonaegui, P., González Clavijo, E.G., Díez Montes, A.D., Rubio Pascual, F.J., Valle Aguado, B.V., 2007. Space and time in the tectonic evolution of the northwestern Iberian Massif. implications for the comprehension of the Variscan belt. Memoir - Geological Society of America 200, 403–423. http://dx.doi.org/10.1130/2007.1200(21).
Martínez-Catalán, J.R., Arenas, R., Abati, J., Martínez, S.S., García, F.D., Suárez, J.F., Cuadra, P.G., Castiñeiras, P., Barreiro, J.G., Montes, A.D., Clavijo, E.G., Pascual, F.J.R., Andonaegui, P., Jeffries, T.E., Alcock, J.E., Fernández, R.D., Carmona, A.L., Sánchez-Martínez, S., Díaz-García, F., Fernández-Suárez, J., González Cuadra, P., Castiñeiras, P., Gómez-Barreiro, J., Díez Montes, A., González Clavijo, E., Rubio Pascual, F.J., Díez Fernández, R., López-Carmona, A., 2009. A rootless suture and the loss of the roots of a mountain chain: the Variscan Belt of NW Iberia. Comptes Rendus Geoscience 341, 114–126. http://dx.doi.org/10.1016/j.crte.2008.11.004.
Martínez-Catalán, J.R., Aerden, D.G.A.M., Carreras, J., 2015. The "Castilian bend" of Rudolf Staub (1926): historical perspective of a forgotten orocline in Central Iberia. Swiss Journal of Geosciences 108, 289–303.
McFadden, P.L., McElhinny, M.W., 1988. The combined analysis of remagnetization circles and direct observations in palaeomagnetism. Earth and Planetary Science Letters 87, 161–172. http://dx.doi.org/10.1016/0012-821X(88)90072-6.
McFadden, P.L., McElhinny, M.W., 1990. Classification of the reversal test in palaeomagnetism. Geophysical Journal International 103, 725–729. http://dx.doi.org/10.1111/j.1365-246X.1990.tb05683.x.
Meijers, M.J.M., van Hinsbergen, D.J.J., Dekkers, M.J., Altıner, D., Kaymakcı, N., Langereis, C.G., 2011. Pervasive Palaeogene remagnetization of the central Taurides fold-and-thrust belt (southern Turkey) and implications for rotations in the Isparta Angle. Geophysical Journal International 184, 1090–1112. http://dx.doi.org/10.1111/j.1365-246X.2010.04919.x.
Merino-Tomé, O.a., Bahamonde, J.R., Colmenero, J.R., Heredia, N., Villa, E., Farias, P., 2009. Emplacement of the Cuera and Picos de Europa imbricate system at the core of the Iberian–Armorican arc (Cantabrian zone, north Spain): New precisions concerning the timing of arc closure. Geological Society of America Bulletin 121, 729–751. http://dx.doi.org/10.1130/B26366.1.
Mullender, T.A.T., Velzen, A.J., Dekkers, M.J., 1993. Continuous drift correction and separate identification of ferrimagnetic and paramagnetic contributions in thermomagnetic runs. Geophysical Journal International 114, 663–672. http://dx.doi.org/10.1111/j.1365-246X.1993.tb06995.x.
Murphy, J.B., Gutierrez-Alonso, G., Nance, R.D., Fernandez-Suarez, J., Keppie, J.D., Quesada, C., Strachan, R.A., Dostal, J., 2006. Origin of the Rheic Ocean: rifting along a Neoproterozoic suture? Geology 34, 325–328. http://dx.doi.org/10.1130/G22068.1.
Murphy, J.B., Nance, R.D., Cawood, P.A., 2009. Contrasting modes of supercontinent formation and the conundrum of Pangea. Gondwana Research 15 (3), 408–420.
Nance, R.D., Gutiérrez-Alonso, G., Keppie, J.D., Linnemann, U., Murphy, J.B., Quesada, C., Strachan, R.A., Woodcock, N.H., 2010. Evolution of the Rheic Ocean. Gondwana Research 17, 194–222. http://dx.doi.org/10.1016/j.gr.2009.08.001.
Nance, R.D., Gutiérrez-Alonso, G., Keppie, J.D., Linnemann, U., Murphy, J.B., Quesada, C., Strachan, R.a., Woodcock, N.H., 2012. A brief history of the Rheic Ocean. Geoscience Frontiers 3, 125–135. http://dx.doi.org/10.1016/j.gsf.2011.11.008.
O'Brien, B.H., 2012. Peri-Gondwanan Arcback–arc Complex and Badger Retroarc Foreland Basin: development of the exploits orocline of Central Newfoundland. Geoscience Canada.
Orejana, D., Villaseca, C., Valverde-Vaquero, P., Belousova, E.A., Armstrong, R.A., 2012. U–Pb geochronology and zircon composition of late Variscan S- and I-type granitoids from the Spanish Central System batholith. International Journal of Earth Sciences 101 (7), 1789–1815.
Pares, J.M., Van der Voo, R., 1992. Paleozoic paleomagnetism of Almaden, Spain: a cautionary note. Journal of Geophysical Research 97, 9353–9356.
Pastor-Galán, D., Gutiérrez-Alonso, G., Weil, A.B., 2011. Orocline timing through joint analysis: insights from the Ibero–Armorican Arc. Tectonophysics 507, 31–46. http://dx.doi.org/10.1016/j.tecto.2011.05.005.
Pastor-Galan, D., Gutierrez-Alonso, G., Zulauf, G., Zanella, F., Pastor-Galán, D., Gutiérrez-Alonso, G., 2012a. Analogue modeling of lithospheric-scale orocline buckling: constraints on the evolution of the Iberian–Armorican Arc. Geological Society of America Bulletin 124, 1293–1309. http://dx.doi.org/10.1130/B30640.1.
Pastor-Galán, D., Gutiérrez-Alonso, G., Mulchrone, K.F., Huerta, P., 2012b. Conical folding in the core of an orocline. A geometric analysis from the Cantabrian Arc (Variscan Belt of NW Iberia). Journal of Structural Geology 39, 210–223. http://dx.doi.org/10.1016/j.jsg.2012.02.010.
Pastor-Galán, D., Martín-Merino, G., Corrochano, D., 2014. Timing and structural evolution in the limb of an orocline: the Pisuerga–Carrión Unit (southern limb of the Cantabrian Orocline, NW Spain). Tectonophysics 622, 110–121. http://dx.doi.org/10.1016/j.tecto.2014.03.004.
Pastor-Galan, D., Groenewegen, T., Brouwer, D., Krijgsman, W., Dekkers, M.J., 2015a. One or two oroclines in the variscan orogen of Iberia? Implications for Pangea amalgamation. Geology 43, 527–530. http://dx.doi.org/10.1130/G36701.1.
Pastor-Galán, D., Ursem, B., Meere, P.A., Langereis, C., 2015b. Extending the Cantabrian Orocline to two continents (from Gondwana to Laurussia). Paleomagnetism from South Ireland. Earth and Planetary Science Letters 432, 223–231.
Perroud, H., Calza, F., Khattach, D., 1991. Paleomagnetism of the Silurian Volcanism at Almaden, Southern Spain. Journal of Geophysical Research 96, 1949–1962.
Pin, C., Paquette, J.L., Ábalos, B., Santos, F.J., Ibarguchi, J.I.G., 2006. Composite origin of an early Variscan transported suture: ophiolitic units of the Morais Nappe Complex (north Portugal). Tectonics 25 (19 PP. doi:200610.1029/2006TC001971).
Quesada, C., 1991. Geological constraints on the Paleozoic tectonic evolution of tectonostratigraphic terranes in the Iberian Massif. Tectonophysics 185 (3–4), 225–245.
Ribeiro, A., 1974. Contribution á l'étude tectonique de Trás-osMontes Oriental. Memórias dos Serviços Geológicos de Portugal 24, 1–168.
Ries, A.C., Shackleton, R.M., 1971. Catazonal complexes of North-West Spain and North Portugal, remnants of a Hercynian thrust plate. Nature Physical Science 234, 65–79.
Rodriguez, J., Cosca, M.A., Ibarguchi, J.I.G., Dallmeyer, R.D., 2003. Strain partitioning and preservation of Ar-40/Ar-39 ages during Variscan exhumation of a subducted crust (Malpica–Tui complex, NW Spain). Lithos 70, 111–139.
Rodriguez-Alonso, M.D., Peinado, M., Lopez-Plaza, M., Franco, P., Carnicero, A., Gonzalo, J.C., 2004. Neoproterozoic–Cambrian synsedimentary magmatism in the Central Iberian Zone (Spain): geology, petrology and geodynamic significance. International Journal of Earth Sciences 93, 897–920.
Rölz, P., 1975. Beiträge zum Aufbau des jungpräkambrischen und altpaläozoischen Grundgebirges in den Provinzen Salamanca und Cáceres (Sierra de Tamames, Sierra de Francia und östliche Sierra de Gata) Spanien (Auszug). Münstersche Forschungen zur Geologie und Paläontologie 36, 1–68.
Rosenbaum, G., 2014. Geodynamics of oroclinal bending: insights from the Mediterranean. Journal of Geodynamics 82, 5–15. http://dx.doi.org/10.1016/j.jog.2014.05.002.

Rosenbaum, G., Li, P., Rubatto, D., 2012. The contorted New England Orogen (eastern Australia): new evidence from U–Pb geochronology of early Permian granitoids. Tectonics 31 (14 PP. doi:201210.1029/2011TC002960).
Rubio Pascual, F.J., Arenas, R., Martínez-Catalán, J.R., Rodríguez Fernández, L.R., Wijbrans, J.R., 2013. Thickening and exhumation of the Variscan roots in the Iberian Central System: tectonothermal processes and $^{40}Ar/^{39}Ar$ ages. Tectonophysics 587, 207–221. http://dx.doi.org/10.1016/j.tecto.2012.10.005.
Schward, E.J., Vaughan, D.J., 1972. Magnetic phase relations of pyrrhotite. Journal of Geomagnetism and Geoelectricity 24, 441–458. http://dx.doi.org/10.5636/jgg.24.441.
Schwarz, E.J., 1974. Magnetic fabric in massive sulfide deposits. Canadian Journal of Earth Sciences 11, 1669–1675. http://dx.doi.org/10.1139/e74-165.
Scotese, C.R., 2001. Atlas of Earth history, volume 1, paleogeography. PALEOMAP Project (Arlington, Texas).
Shaw, J., Johnston, S.T., 2016. Terrane wrecks (coupled oroclines) and paleomagnetic inclination anomalies. Earth-Science Reviews 154, 191–209. http://dx.doi.org/10.1016/j.earscirev.2016.01.003.
Shaw, J., Johnston, S.T., Gutiérrez-Alonso, G., Weil, A.B., 2012. Oroclines of the Variscan orogen of Iberia: paleocurrent analysis and paleogeographic implications. Earth and Planetary Science Letters 329–330, 60–70. http://dx.doi.org/10.1016/j.epsl.2012.02.014.
Shaw, J., Gutiérrez-Alonso, G., Johnston, S.T., Galán, D.P., 2014. Provenance variability along the Early Ordovician north Gondwana margin: paleogeographic and tectonic implications of U–Pb detrital zircon ages from the Armorican Quartzite of the Iberian Variscan belt. Geological Society of America Bulletin 126 (5–6), 702–719.
Shaw, J., Johnston, S.T., Gutiérrez-Alonso, G., 2016. Orocline formation at the core of Pangea: a structural study of the Cantabrian orocline, NW Iberian Massif. Lithosphere 8, 97.
Stampfli, G.M., Borel, G.D., 2002. A plate tectonic model for the Paleozoic and Mesozoic constrained by dynamic plate boundaries and restored synthetic oceanic isochrons. Earth and Planetary Science Letters 196, 17–33. http://dx.doi.org/10.1016/S0012-821X(01)00588-X.
Stampfli, G.M., Hochard, C., Vérard, C., Wilhem, C., VonRaumer, J., 2013. The formation of Pangea. Tectonophysics 593, 1–19. http://dx.doi.org/10.1016/j.tecto.2013.02.037.
Staub, R., 1926. Gedanken zum Strukturbild Spaniens. XIV Congrès Géologique International 3, 949–996.
Tait, J.A., Bachtadse, V., Soffel, H., 1996. Eastern Variscan fold belt: paleomagnetic evidence for oroclinal bending. Geology 24, 871–874.
Tauxe, L., 2010. Essentials of Paleomagnetism.
Tauxe, L., Watson, G.S., 1994. The fold test: an eigen analysis approach. Earth and Planetary Science Letters 122, 331–341. http://dx.doi.org/10.1016/0012-821X(94)90006-X.
Thomas, W.A., 1977. Evolution of Appalachian–Ouachita salients and recesses from reentrants and promontories in the continental margin. American Journal of Science 277, 1233–1278. http://dx.doi.org/10.2475/ajs.277.10.1233.
Torsvik, T.H., Van der Voo, R., Preeden, U., Niocaill, C.M., Steinberger, B., Doubrovine, P.V., van Hinsbergen, D.J.J.J., Domeier, M., Gaina, C., Tohver, E., Meert, J.G., McCausland, P.J.a.A., Cocks, L.R.M., Mac Niocaill, C., Steinberger, B., Doubrovine, P.V., van Hinsbergen, D.J.J.J., Domeier, M., Gaina, C., Tohver, E., Meert, J.G., McCausland, P.J.a.A., Cocks, L.R.M., 2012. Phanerozoic polar wander, palaeogeography and dynamics. Earth-Science Reviews 114, 325–368. http://dx.doi.org/10.1016/j.earscirev.2012.06.007.
Valladares, M.I., Barba, P., Ugidos, J.M., Colmenero, J.R., Armenteros, I., 2000. Upper Neoproterozoic–Lower Cambrian sedimentary successions in the Central Iberian Zone (Spain): sequence stratigraphy, petrology and chemostratigraphy. Implications for other European zones. International Journal of Earth Sciences 89, 2–20.
Valverde-Vaquero, P., Díez Balda, M.A., Díez Montes, A., Dörr, W., Escuder-Viruete, J., González-Clavijo, E., Maluski, H., Rodríguez-Fernández, L.R., Rubio, F., Villar, P., 2007. The "hot orogeny": two separate variscan low-pressure metamorphic events in the Central Iberian Zone. In: Faure, M., Lardeaux, J.-M., Ledru, P., Peschler, A., Schulmann, K. (Eds.), Mechanics of Variscan Orogeny: a Modern View on Orogenic ResearchGéologie de la France 2007 2. Societe´ Géologique de France and Bureau de Recherches Géologiques et Minières, p. 168.
van der Voo, R., 2004. Paleomagnetism, oroclines, and growth of the continental crust. GSA Today 5173, 4–11. http://dx.doi.org/10.1130/1052-5173(2004)014<4.
van der Voo, R., Stamatakos, J.A., Pares, J.M., 1997. Kinematic constraints on thrust-belt curvature from syndeformational magnetizations in the Lagos del Valle Syncline in the Cantabrian Arc, Spain. Journal of Geophysical Research - Earth 102, 10105–10119.
van Hinsbergen, D.J.J., Dekkers, M.J., Koç, A., 2010. Testing Miocene remagnetization of bey Dağları: timing and amount of Neogene rotations in SW Turkey. Turkish Journal of Earth Sciences 19, 123–156.
Villaseca, C., Orejana, D., Belousova, E., Armstrong, R.A., Pérez-Soba, C., Jeffries, T.E., 2011. U–Pb isotopic ages and Hf isotope composition of zircons in Variscan gabbros from central Spain: evidence of variable crustal contamination. Mineralogy and Petrology 101 (3–4), 151–167.
Viruete, J.E., Indares, A., Arenas, R., 2000. P–T paths derived from garnet growth zoning in an extensional setting: an example from the Tormes Gneiss Dome (Iberian Massif, Spain). Journal of Petrology 41 (10), 1489–1515.
Weil, A.B., Sussman, A.J., 2004. In: Sussman, A.J., Weil, A.B. (Eds.), Classifying curved orogens based on timing relationships between structural development and vertical-axis rotations. Geological Society of America, pp. 1–16.
Weil, A.B., Van der Voo, R., van der Pluijm, B.A., Pares, J.M., 2000. The formation of an orocline by multiphase deformation: a paleomagnetic investigation of the Cantabria-Asturias Arc (northern Spain). Journal of Structural Geology 22, 735–756.
Weil, A.B., van der Voo, R., van der Pluijm, B.A., 2001. Oroclinal bending and evidence against the Pangea megashear: the Cantabria–Asturias arc (northern Spain). Geology 29, 991–994.
Weil, A.B., Gutiérrez-Alonso, G., Conan, J., 2010. New time constraints on lithospheric-scale oroclinal bending of the Ibero–Armorican Arc: a paleomagnetic study of earliest Permian rocks from Iberia. Journal of the Geological Society of London 167, 17. http://dx.doi.org/10.1144/0016-76492009-002.
Weil, A.B., Gutiérrez-Alonso, G., Johnston, S.T., Pastor-Galán, D., 2013. Kinematic constraints on buckling a lithospheric-scale orocline along the northern margin of Gondwana: a geologic synthesis. Tectonophysics 582, 25–49. http://dx.doi.org/10.1016/j.tecto.2012.10.006.
Weltje, G.J., 1997. End-member modeling of compositional data: numerical–statistical algorithms for solving the explicit mixing problem. Mathematical Geology 29, 503–549. http://dx.doi.org/10.1007/BF02775085.
Wise, D.U., 2004. Pennsylvania salient of the Appalachians: a two-azimuth transport model based on new compilations of Piedmont data. Geology 32, 777. http://dx.doi.org/10.1130/G20547.1.
Yenes, M., Álvarez, F., Gutiérrez-Alonso, G., 1999. Granite emplacement in orogenic compressional conditions: the La Alberca–Béjar granitic area (Spanish Central System, Variscan Iberian Belt). Journal of Structural Geology 21 (10), 1419–1440.
Zeck, H.P., Wingate, M.T.D., Pooley, G., 2007. Ion microprobe U–Pb zircon geochronology of a late tectonic granitic–gabbroic rock complex within the Hercynian Iberian belt. Geological Magazine 144 (01), 157–177.
Zijderveld, J.D.A., 1967. A.C. demagnetization of rocks: analysis of results. In: Collisnson, D., Creer, K., Runcorn, S. (Eds.), Methods of Paleomagnetism. Elsevier, Amsterdam, pp. 254–286.